

This work was written as part of one of the author's official duties as an Employee of the United States Government and is therefore a work of the United States Government. In accordance with 17 U.S.C. 105, no copyright protection is available for such works under U.S. Law.

Public Domain Mark 1.0

<https://creativecommons.org/publicdomain/mark/1.0/>

Access to this work was provided by the University of Maryland, Baltimore County (UMBC) ScholarWorks@UMBC digital repository on the Maryland Shared Open Access (MD-SOAR) platform.

Please provide feedback

Please support the ScholarWorks@UMBC repository by emailing scholarworks-group@umbc.edu and telling us what having access to this work means to you and why it's important to you. Thank you.

Characterization of the optical properties of biomass burning aerosols in Zambia during the 1997 ZIBBEE field campaign

T. F. Eck,^{1,2} B. N. Holben,³ D. E. Ward,⁴ O. Dubovik,⁵ J.S. Reid,⁶ A. Smirnov,⁵ M. M. Mukelabai,⁷ N.C. Hsu,⁵ N. T. O'Neill,⁸ and I. Slutsker⁵

Abstract. The physical and optical properties of biomass burning aerosols in a savanna region in south central Africa (Zambia) were analyzed from measurements made during the Zambian International Biomass Burning Emissions Experiment (ZIBBEE) during August–September 1997. Due to the large spatial extent of African savannas and the high frequency of occurrence of burning in the annual dry seasons, characterization of the optical properties of the resultant biomass burning aerosols is important for the study of atmospheric radiative processes and for remote sensing of both surface and atmospheric properties in these regions. Aerosol Robotic Network Sun-sky radiometer spectral measurements of direct Sun observations and directional sky radiances were utilized to infer spectral aerosol optical depths (τ_a), aerosol size distributions, and single-scattering albedos. During the primary ZIBBEE study period, which coincided with the peak period of biomass burning in the region, there was a high correlation between the measured τ_a and the total column water vapor or precipitable water vapor (PWV), suggesting transport of smoke aerosol from regions with higher PWV. Size distribution retrievals of the biomass burning smoke show that the accumulation mode dominated and a comparison with smoke from Amazonia (Bolivia) shows a shift toward smaller particles for African savanna smoke. This may be the result of differences in mode of combustion (flaming versus smoldering), fuel type and moisture content, and the aging processes of the aerosol. The single-scattering albedo (ω_0) of the aerosols were retrieved using several approaches, yielding average values of ω_0 at ~ 550 nm during ZIBBEE varying from ~ 0.82 to ~ 0.85 , thus showing good agreement within the retrieval uncertainty of ~ 0.03 of these methods. In general, ω_0 was relatively constant as a function of aerosol loading, with very little change occurring for τ_a at 440 nm ranging from 0.7 to 1.7. African savanna smoke exhibits significantly higher absorption than smoke from Amazonian forested regions and also a greater rate of decrease of ω_0 with increasing wavelength. Variations in the spectral change of the Ångström wavelength exponent were also investigated with respect to the degree of aerosol absorption and changes in the accumulation mode size distributions.

1. Introduction

Biomass burning, and the resultant production of aerosols containing black carbon, occurs primarily in the tropical and subtropical regions of the globe [Dwyer *et al.*, 1998; Levine *et al.*, 1995]. Dwyer *et al.* [1998] have utilized advanced very high resolution radiometer (AVHRR) satellite data to globally

map the distribution of remotely sensed fires and found that 80% occur in the tropics with Africa having the largest number of fires of all continents. Fires in savanna ecosystems consume more dry biomass per year than fires in other ecosystems [Levine *et al.*, 1995], and Africa contains two thirds of the Earth's savanna area.

Analysis of fire pixel counts from AVHRR remote sensing shows a significant interannual variability and differences in seasonality for the various biomass burning regions of Africa [Cooke *et al.*, 1996]. Interannual variability in fire seasonality resulting from variability in meteorological conditions consequently results in variable concentrations of biomass burning aerosols during the dry season and between dry seasons. Sun photometer measurements of aerosol optical depth τ_a from Aerosol Robotic Network (AERONET) instruments [Holben *et al.*, 1998] have been made in the miombo woodland savanna region of west central Zambia since 1995. Analysis of these data [Holben *et al.*, 2001] has shown interannual variation in τ_a during the principal burning months of August through November. For example, the monthly mean τ_a in November was observed to vary by more than a factor of 2 during the 1995–1998 time period. This variability may possibly be due to differences in the onset of the wet season which directly impacts the number of fires,

¹Raytheon ITSS, NASA Goddard Space Flight Center, Greenbelt, Maryland.

²Now at Goddard Earth Sciences and Technology Center, University of Maryland, Baltimore County, Baltimore, Maryland.

³Biospheric Sciences Branch, NASA Goddard Space Flight Center, Greenbelt, Maryland

⁴Intermountain Research Station, USDA Forest Service, Missoula, Montana.

⁵Science Systems and Applications, Inc., NASA Goddard Space Flight Center, Greenbelt, Maryland.

⁶Atmospheric Propagation Branch, Space and Naval Warfare Systems Center, San Diego, California.

⁷Zambian Meteorological Department, Mongu, Zambia.

⁸Centre d'Applications et de Recherches en Teledetection, Université de Sherbrooke, Quebec, Canada.

Copyright 2001 by the American Geophysical Union.

Paper number 2000JD900555.
0148-0227/01/2000JD900555\$09.00

and/or also due to differences in atmospheric circulation which result in differences in the amount of biomass burning aerosols transported from various source regions. Nearly all fires in the African savannas result from human activity. Human population pressure is increasing the extent of burning over the recent historical time period [Goldammer, 1991]. Analysis of remotely sensed absorbing aerosols from TOMS satellite sensors by Hsu *et al.* [1999] for the 20 year period of 1979–1998 has shown a trend of increasing smoke τ_a at 380 nm with time over the west central Zambia region. This increasing trend may be due in part to increases in human population and concurrent increases in land use for agriculture; however, the trend may also be due to decadal scale climatic variations such as in the timing and extent of rainfall over the region.

Wild [1999] has shown that a lack of adequate seasonally resolved aerosol climatologies over biomass burning regions of Africa has resulted in large uncertainties in general circulation model (GCM) calculations of atmospheric shortwave absorption due to absorbing aerosols from vegetation fires. The analysis of Konzelmann *et al.* [1996] has shown that for biomass burning regions of Africa the differences between satellite-estimated and surface-measured total shortwave incident solar radiation ranged from 25 to 40% and may be due to the radiative effects of biomass burning aerosols. In addition to characterization of both the direct and the indirect radiative forcing effects of the African biomass burning aerosols, it is also important to have an accurate knowledge of regional aerosol radiative characteristics in order to enable more accurate remote sensing of Earth surface and atmospheric characteristics.

In August–September 1995 the Smoke, Clouds, and Radiation – Brazil (SCAR-B) experiment was conducted in the Brazilian Amazon, and this resulted in detailed and extensive characterization of biomass burning aerosol optical properties for this region [Kaufman *et al.*, 1998]. Relatively little information has been published on the optical properties of biomass burning aerosols in Africa. However, recent research in southern Africa and Brazil have demonstrated large differences in burning characteristics between fires in savanna ecosystems and fires associated with deforestation. In both Brazil and Africa, Ward *et al.* [1996] and Ward *et al.* [1992] have found that nearly 85% of the biomass was consumed through flaming combustion for savanna ecosystems, whereas for deforestation fires 50% or less of the biomass was consumed through flaming combustion. They also found that as much as 15 to 20% of the aerosol produced was black carbon for flaming combustion compared to less than 3% for smoldering combustion. These differences in combustion phase may result in large differences in the absorption characteristics of smoke produced from fires in differing ecosystems.

In this paper we present some of the observations of biomass burning aerosols made in the savanna burning region of western Zambia in August–September 1997, as a part of the Zambian International Biomass Burning Emission Experiment (ZIBBEE). The ZIBBEE field campaign was organized in cooperation with the U.S. Forest Service Fire Chemistry Lab, the Zambian Meteorology Department, and NASA's AERONET project. The primary objectives were to quantify the aerosol and trace gas fluxes from the savannas and woodlands of southern Africa. Embedded within this study are objectives to

quantify the consumption of biomass (carbon) from biomass burning, validate aerosol retrievals from various satellite sensors, and investigate direct radiative forcing by biomass burning aerosols. The SAFARI 2000 dry season field campaign, which was conducted in southern Africa in August–September 2000, will provide many more observations of aerosol properties in this region, resulting in a more complete characterization.

2. Study Region, Instrumentation, and Methodology

2.1. Region of Study

The three sites on which we focus most of our analysis in this paper are Mongu (15° 15' S, 23° 09' E), Zambezi (13° 31' S, 23° 06' E), and Senanga (16° 06' S, 23° 06' E), which are located in a nearly north-south transect of western Zambia, adjacent to the floodplain of the Zambezi River. They range in altitude from 1025 to 1107 m above sea level, as most of Zambia and some areas of adjacent countries are located on an elevated plateau. There is a pronounced wet and dry period seasonality in western Zambia, with the 7 month dry season of April–October in Mongu having less than 8% of the mean annual total precipitation of 969 mm. The principal vegetative cover in western Zambia is miombo woodland savanna, with some grassland savanna, and cropland and seasonal marshes in the river floodplains. Grasses growing between the miombo trees (canopy coverage is incomplete) account for much of the biomass fuel burned in the woodland savanna regions. The time period of the ZIBBEE experiment, late August through September, coincides with the peak periods of agricultural burning and thus the highest levels of τ_a for biomass burning aerosols. Subsidence from anticyclonic circulation is a dominant meteorological feature during much of the biomass burning season in this region with four stable vertical layers identified in the troposphere [Garstang *et al.*, 1996]. This atmospheric stability often results in cloudless or nearly cloudless sky conditions for extended periods at this time of the year. However, 1997 was a year with one of the strongest El Niño events on record, and there were some unusually early rainfall events that occurred in the second week of September 1997.

2.2. Instrumentation

All of the CIMEL Electronique CE-318 Sun-sky radiometer measurements reported in this paper were made with instruments that are a part of the AERONET global network. These instruments are described in detail by Holben *et al.* [1998]; however, a brief description will be given here. The automatic tracking Sun and sky scanning radiometers made direct Sun measurements with a 1.2° full field of view every 15 min at 340, 380, 440, 500, 675, 870, 940, and 1020 nm (nominal wavelengths). The direct Sun measurements take ~8 s to scan all eight wavelengths, with a motor-driven filter wheel positioning each filter in front of the detector. These solar extinction measurements are then used to compute aerosol optical depth at each wavelength except for the 940 nm channel, which is used to retrieve total precipitable water in centimeters. The filters utilized in these instruments were ion-assisted deposition interference filters with a band pass (full

width at half maximum) of the 340 nm channel at 2 nm and the 380 nm filter at 4 nm, while the bandpass of all other channels was 10 nm. Calibration of field instruments was performed by a transfer of calibration from reference instruments that were calibrated by the Langley plot technique at Mauna Loa Observatory (MLO), Hawaii. Reference instruments are typically calibrated at MLO every 2–3 months using morning measurements only. The inter calibration of field instruments was performed both pre-deployment and post-deployment at Goddard Space Flight Center (GSFC), and a linear change in calibration with time was assumed in the interpolation between the two calibrations. The combined effects of uncertainties in calibration, atmospheric pressure (not monitored), and total ozone amount (climatology is used) result in a total uncertainty of ~ 0.010 – 0.021 in computed τ_a for field instruments (which is spectrally dependent with the higher errors in the UV [Eck *et al.*, 1999]). The effect of forward scattered diffuse radiation within the 1.2° field of view of the Sun photometer has also been considered. Simulations by Kinne *et al.* [1997] show that for aerosol particles with an effective radius of $0.2 \mu\text{m}$ (similar in size to biomass burning aerosols), there is essentially no measured effect on aerosol optical depth, even for Sun photometers with a 2° field of view. Schmid *et al.* [1999] compared τ_a values derived from four different solar radiometers (one was an AERONET Sun-sky radiometer) operating simultaneously together in a field experiment and found that the τ_a values from 380 to 1020 nm agreed to within 0.015 (rms), which is similar to our estimated level of uncertainty in τ_a retrieval for field instruments.

In Mongu, measurements of broadband photosynthetically active radiation (PAR; 400–700 nm) fluxes were made with a Skye-Probetech SKE-510 instrument. These measurements of PAR flux were made at 1 min sampling intervals, and the data were transmitted to the Meteosat satellite along with the CIMEL Sun-sky radiometer data. To investigate the repeatability of the calibration of the PAR flux sensors, we compared simultaneous measurements made with five Skye Probetech SKE-510 sensors and with an Optronic OL 754 spectroradiometer. The Optronic spectroradiometer instrument measured spectral flux from 300 to 800 nm at 10 nm intervals with a 2 nm band pass. Spectral integration from 400 to 700 nm was performed in order to compute broadband PAR flux from the Optronic instrument. A comparison of the measured PAR fluxes from all six instruments under cloudless conditions at GSFC on July 31, 1997, at 1429 UT (41.3° solar zenith angle) is shown in Table 1. The aerosol optical depth on this date and time was representative of clean background conditions for summer at GSFC with a low τ_{a500} value of 0.08. Two solar irradiance models were utilized to compute the PAR flux at this solar zenith angle with CIMEL-retrieved τ_a and PWV data used as input. For the SPCTRAL2 model [Bird and Riordan, 1986] we assumed a value for the asymmetry factor g of 0.60 and ω_0 of 0.90. For the 6S model [Vermote *et al.*, 1997] we assumed refractive indices which yielded a single-scattering albedo value of 0.90 and assumed two different aerosol size distributions. The 6S model is a radiative transfer model that relies on the successive order of scattering method and therefore is not related to any radiance sources used in the calibration of flux-measuring instruments. Both models (6S and SPCTRAL2) use the extraterrestrial solar flux data of Neckel and Labs [1981]. The sensitivity of the computation of PAR flux from the 6S spectral model, for this low τ_a case, to

Table 1. Comparison of Measured Versus Modeled PAR (400–700 nm) Flux at GSFC on July 31, 1997, at 1429 UT (Solar Zenith= 41.3°), When CIMEL-Measured τ_{a500} was 0.08

Model or Flux Instrument Type	Measured or Modeled PAR Flux (W/m^2)	Percentage Difference Versus Model Average
6S model	341.9	
SPCTRAL2 model	339.2	
Average of above two models	340.6	
Skye-Probetech SKE-510 13986	335.7	-1.42
Skye-Probetech SKE-510 13984	329.7	-3.19
Skye-Probetech SKE-510 3363	346.6	1.78
Skye-Probetech SKE-510 3362	353.7	3.86
Skye-Probetech SKE-510 8790	321.8	-5.51
Optronic OL 754 Spectrally integrated	331.4	-2.69

varying ω_0 from 0.85 to 0.95 was only $\sim 0.6\%$, to varying the size distribution model from the urban/industrial dynamic model of Remer *et al.* [1998] to the 6S continental aerosol model was only $\sim 0.1\%$, for varying the PWV amount by 20% was only $\sim 0.15\%$, for varying τ_a by 0.01 was only $\sim 0.3\%$, and for varying the surface reflectance from sand to vegetation representative values was only $\sim 0.25\%$. Therefore any assumptions made about the aerosol optical or surface reflectance characteristics under such a low aerosol loading resulted in an uncertainty in 6S-computed PAR fluxes of $<1\%$. The computed PAR flux for both the 6S and the SPCTRAL2 models differed by only $\sim 0.8\%$ for this case, and we used the average PAR flux from the two models to compare to the measured PAR fluxes. Measurements of the PAR flux from the five Skye-Probetech sensors versus the modeled flux differed by amounts that varied from $+3.9\%$ to -5.5% . This is within the stated absolute calibration accuracy given by the manufacturer (“typically 3%, 5% maximum”). The Optronic spectroradiometer integrated value of PAR flux differed from the modeled flux by $\sim 2.7\%$. To standardize the measured PAR fluxes from all five Skye-Probetech instruments, we computed the ratio of the measured flux to the modeled flux for each instrument for this intercomparison date and time and utilized this ratio as a multiplier along with the original calibration coefficient for data at all other dates and times.

2.3. Analysis Methodology

The CIMEL sky radiance almucantar measurements at 440, 675, 870, and 1020 nm in conjunction with the direct Sun-measured τ_a at these same wavelengths were used to retrieve aerosol size distributions following the methodology of Dubovik *et al.* [2000]. Almucantar sky radiance measurements were made at optical air masses of 4, 3, and 2 in the morning

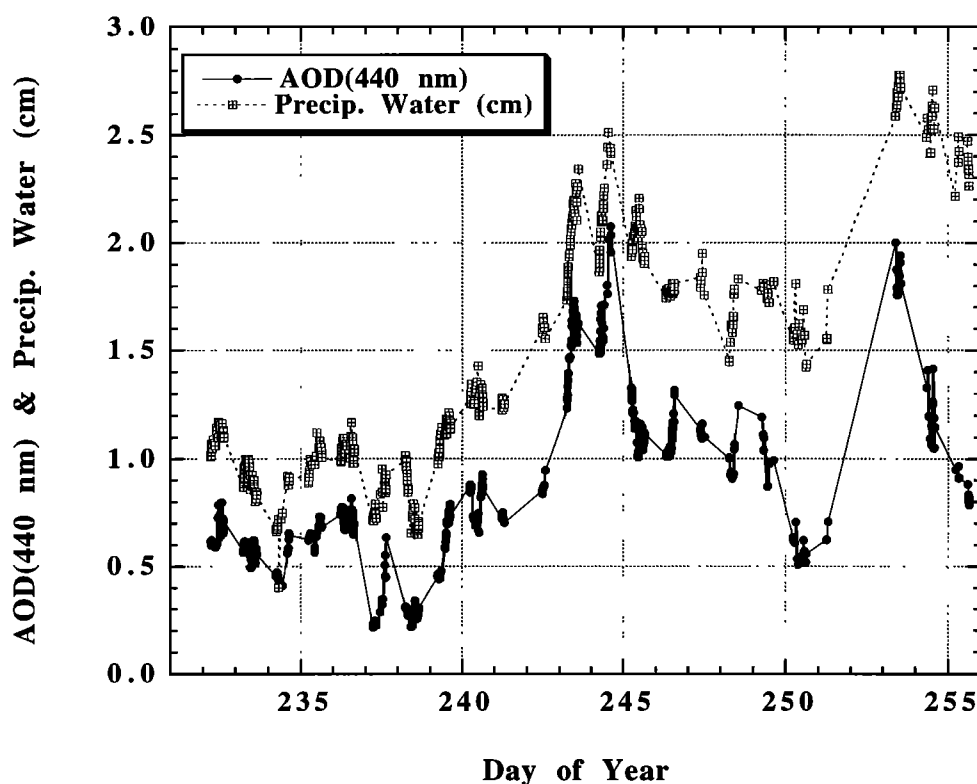


Figure 1. Time series of instantaneous measurements of precipitable water vapor (PWV) and aerosol optical depth (AOD) at 440 nm in Mongu, Zambia, from August 20 (day 232) to September 12 (day 255), 1997.

and afternoon, and once per hour in between. Spherical particle shape is assumed in the retrievals; a reasonable assumption for smoke aerosol as the measurements of *Martins et al.* [1998] showed that particles in Amazonian regional smoke hazes were largely spherical. Sensitivity studies performed by *Dubovik et al.* [2000] were used to analyze the perturbations of the inversion resulting from random errors, possible instrument offsets, and known uncertainties in the atmospheric radiation model. Retrieval tests using known size distributions demonstrated successful retrievals of mode radii and the relative magnitude of modes for various types of size distributions such as bimodal accumulation mode dominated aerosols and bimodal coarse mode dominated aerosols. Simultaneous retrievals of aerosol single-scattering albedo are also made with this algorithm, and the sensitivity analysis shows that these retrievals have an uncertainty of ~ 0.03 – 0.05 depending on aerosol type and aerosol optical depth [*Dubovik et al.*, 2000].

3. Temporal and Spatial Variability of τ_a

Knowledge of the spatial and temporal variability of aerosol optical depth is important for achieving a better understanding of the production and transport of biomass burning aerosols in the region. In addition, this information is important in evaluating satellite retrievals of τ_a since some sensors have large fields of view, and others have retrievals that are effective only over low reflectance targets, which may be widely separated in space. Also, comparisons of spatial variance estimated from satellite retrievals versus ground-based assessments are needed in order to verify that the

satellite-measured variability in τ_a is due to aerosol alone and not also due to surface characteristics variability.

The variation in time of τ_a and total column-integrated precipitable water vapor (PWV) in centimeters at Mongu, Zambia, for a 24 day period during ZIBBEE (August 20 to September 12) is shown in Figure 1. This is the primary time period of the ZIBBEE experiment, when most of the CIMEL Sun photometers were operating at all monitored sites. Large variations in the instantaneous magnitudes of τ_{a440} and PWV are noted with τ_{a440} ranging from a minimum of ~ 0.20 to a maximum of ~ 2.1 , while PWV ranges from ~ 0.7 to ~ 2.8 cm. These data have been screened for clouds, following the methodology of *Smirnov et al.* [2000a]. A high level of coherence is noted between the time series of τ_{a440} and the PWV, and indeed the correlation coefficient for a linear fit is very high, with $r^2 = 0.76$. It is unlikely that there was a large change in particle size (and thus τ_a) due to aerosol hygroscopic growth since *Kotchenruther and Hobbs* [1998] report that for biomass burning aerosols in Amazonia, there were relatively weak increases in light-scattering coefficient as relative humidity increased. Therefore this high correlation suggests possible transport of aerosols from source regions where water vapor is also greater and, conversely, transport of cleaner lower τ_a air from regions which are also drier. Similarly, *Remer et al.* [1998] found a correlation between biomass burning τ_a and PWV in the savanna regions of Brazil ($r = 0.59$), which was due in part to higher levels of biomass and thus greater smoke production to the north in Amazonian tropical forest regions, where PWV is also higher. It is again noted that one of the strongest El Niño events on record occurred in 1997, resulting in some early rain events in

September, so meteorological conditions during ZIBBEE may not in all respects be representative of non-El Niño years.

Plate 1 shows values of the aerosol index (AI) from the Total Ozone Mapping Spectrometer (TOMS) instrument on the Earth Probe satellite for August 23–26, 1997, with 700 mbar streamline analysis from the National Meteorological Center (NMC) superimposed for the southern Africa region. The geopotential heights of the 700 mbar streamlines are ~3100 m, while the altitude of the plateau is ~1100 m at Mongu; thus the streamlines are representative of the wind field at ~2 km above the surface at Mongu and much of Zambia. Note that the wind vector arrow lengths in Plate 1 are proportional to the magnitude of the wind speed. The white areas on the TOMS AI maps represent data gaps between orbits. Hsu *et al.* [1999] found the TOMS aerosol index to be highly correlated with AERONET measurements of $\tau_{a,380}$ for Mongu ($r = 0.86$) for the biomass burning season months of July–October 1996 and 1997. On August 26, 1997 (day 238), the TOMS aerosol index is low (<0.50) at Mongu (black triangle near map center), the wind flow at 700 mbar is from the east-southeast (Plate 1), and this is the day of lowest τ_a and PWV in Figure 1. It is also observed on this day that the maximum values of TOMS AI are to the north, west, and south of Mongu with transport occurring in counterclockwise flow around the atmospheric high and aerosol is advected over the Cape of Good Hope and into the Indian Ocean. Plate 2 shows TOMS AI/ NMC streamline maps for August 31 to September 3, 1997, when AI, τ_a , and PWV were higher over Mongu. Examination of the wind vectors for August 31 (day 243) shows a weak flow with a northerly component. These cases suggest that the high correlation between τ_a and PWV seen in Figure 1 results at least in part from changes in atmospheric circulation with high τ_a and PWV associated with a northerly flow component, while air with low τ_a and PWV is associated with a southerly flow component. Remote sensing satellite retrievals of PWV from HIRS2/MSU data for Africa for September 5, 1988 [Justice *et al.*, 1991], show a general north to south gradient in decreasing PWV amount over the south central Africa region.

Estimates of the amount of biomass burned in southern Africa by Scholes *et al.* [1996], which utilized burned area estimates from satellite measurements [Justice *et al.*, 1996] showed a strong north-south gradient (higher in the north) primarily due to a north-south gradient in rainfall and thus a north-south gradient in vegetation production. In addition, the fire pixel counts measured by AVHRR [Justice *et al.*, 1996] show many more fires north of central Zambia and relatively few fires south of the Zambian border for August 16 to October 15, in both 1992 and 1989. The frequency of occurrence of high aerosol loading, as measured by TOMS AI, also showed a north-south gradient [Herman *et al.*, 1997] with the most prevalent areas of heavy smoke to the north of Zambia in August and September. Analysis of trajectories over southern Africa by Garstang *et al.* [1996] identified five modes of aerosol transport which are likely to occur, with transport possible in all major directions both from and to western Zambia. It is noted that enhanced meteorological observations (more upper air balloon soundings) plus enhanced satellite remote sensing measurements (MODIS and MISR sensors on the TERRA satellite) will be available for the August–September 2000 South African Regional Science Initiative (SAFARI 2000) dry season campaign. This will allow a more

thorough and complete analysis of aerosol transport than presented in the current paper. In addition, measurements of aerosol hygroscopicity of the African smoke during SAFARI 2000 will give a clearer understanding of the relative growth of fine mode particle size due to relative humidity variability.

Although there is a very high correlation between τ_a and PWV in Mongu for the period August 20 to September 12, 1997 (Figure 1), it is noted that the correlation decreases significantly when the period of time analyzed is lengthened significantly. Holben *et al.* [2001] analyzed multiyear (1995–1998) daily mean τ_a and PWV for June through December and found a very low correlation ($r = 0.01$) between τ_a and PWV. This low correlation is due in a large part to many occurrences of low τ_a and high PWV in November and December when PWV is high throughout the region and the rainy season has commenced, resulting in aerosol washout and less burning.

Smoke τ_a values for this time period exhibited a high degree of temporal variability (Figure 1). For example, the autocorrelation coefficients for the Mongu site were 0.45, -0.21, and -0.0 for 1, 2, and 3 day lags, respectively. Zambezi and Senanga had similar autocorrelation coefficients as well. Given that the cutoff for statistical significance was 0.48 ($p < 0.05$), the autocorrelation coefficients for these sites are not even significant after 1 day. This reflects the dependence of the burning/transport relationship on large-scale synoptic meteorology patterns.

The spatial variance of τ_a in western Zambia along a nearly north-south transect, following the Zambezi River floodplain, was also investigated. The three CIMEL instruments deployed in Mongu, Senanga, and Zambezi, Zambia, were located at distances ranging from 96 km apart (Mongu - Senanga) to 276 km apart (Zambezi - Senanga). Figure 2 shows the variation in time of instantaneous values of τ_a at 500 nm at these three sites for the time period of August 27 to September 12, 1997, when all instruments were operating (except for Zambezi on September 11 and 12). The data in this figure have been screened for clouds by setting a threshold of Ångström wavelength exponent (α) of >1.6 , with α being computed from τ_a at 440 and 870 nm. Holben *et al.* [2001] found mean monthly average values of α to be >1.7 for the months of June through October, which is typical of biomass burning aerosols dominated by accumulation mode sized particles [Eck *et al.*, 1999]. The use of the α threshold for cloud screening in this analysis was chosen so that temporally variable smoke plumes would not be eliminated from the data set. For smoke aerosol dominated by fine mode particles it is possible to use the magnitude α as a potential measure of cloud contamination, while in general, for many locations and seasons, making an a priori assumption on the magnitude of α is problematic due to the unknown or variable nature of the aerosol size distribution.

It is noted that the day-to-day variability in τ_a for this 17 day period (Figure 2) is quite similar for all three sites, thus suggesting that similar meteorological conditions are affecting both the transport of aerosols and the burning conditions within this area. In addition, there was often a large variability of τ_a within a day at a given site, and this diurnal variability was sometimes similar for all three sites. The correlation coefficients (r) computed from linear regressions of τ_a for station pairs are shown in Figure 3 for three wavelengths: 675, 500, and 380 nm. These data were time matched, so the difference in time between data acquired for

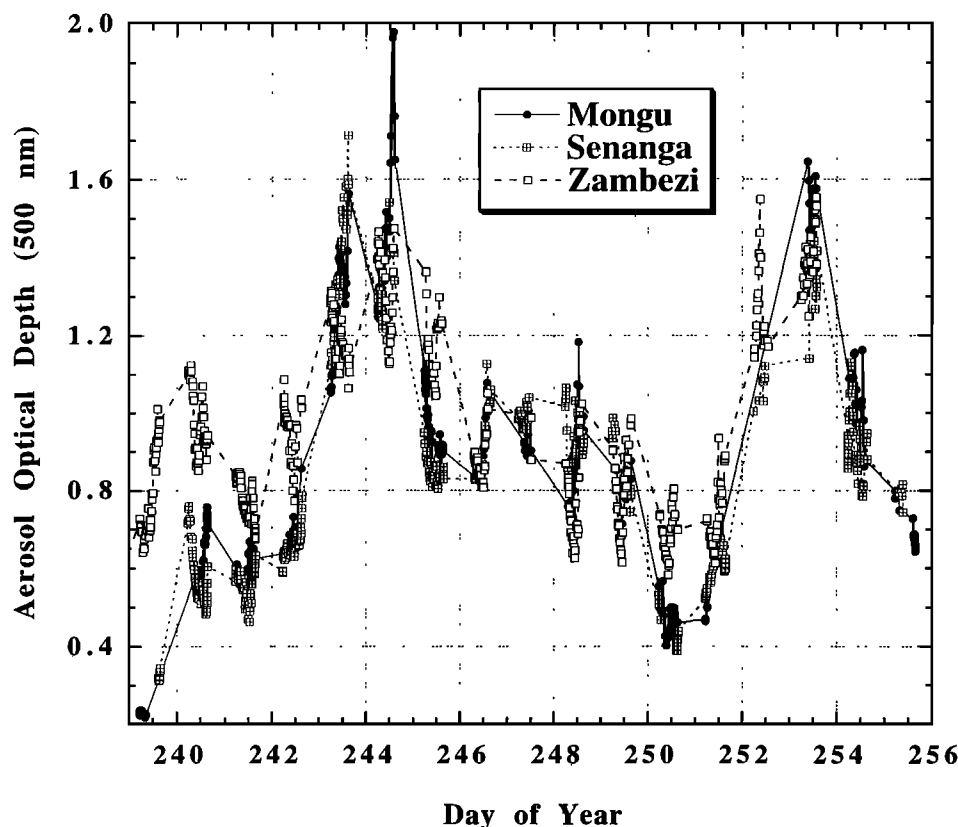


Figure 2. Time series of instantaneous measurements of aerosol optical depth at 500 nm for three sites in western Zambia for August 27 to September 12, 1997. Senanga is located ~95 km nearly directly south of Mongu, and Zambezi is located ~180 km nearly directly north of Mongu.

each pair of stations was 3 min or less, in order to approximate the observations that a satellite sensor would make with simultaneous measurements over a region. There was a nearly linear decrease in correlation between τ_a at these sites as distance between the sites increased. Additionally, there was greater spectral divergence in correlation as distance increased (with lower correlation at shorter wavelengths), due to greater dynamic variability in τ_a at shorter wavelengths than at longer wavelengths. This occurs as a result of the dominance of accumulation mode sized particles (discussed in detail in section 4) and the greater sensitivity of τ_a at shorter wavelengths to changes in particle size and absorption resulting from variations in combustion conditions and/or aging of the particles [Reid *et al.*, 1999]. The mean differences in spectral τ_a between station pairs for time coincident observations (<3 min) is shown in Figure 4. The differences between τ_a of station pairs at all three distance combinations were made by subtracting the more southerly station values from the more northerly station values and computing the mean of these instantaneous values over the time period. Thus since all the mean difference values in Figure 4 are positive, this indicates that there was, in general, a north-south gradient in τ_a with higher τ_a in the north. The instantaneous differences were not all positive however, with for example, the differences for Mongu – Senanga τ_a at 380 nm ranging from ~0.55 (higher in the north) to ~-0.35 (higher in the south), while the mean difference was 0.088 and the mean absolute value difference was 0.121. The distance between the Mongu –

Senanga station pair of 96 km is similar to the spatial scale of the pixel size of the TOMS instrument on Nimbus 7, and thus these spatial variance data help to characterize the variability which can be expected within a pixel for this region.

The spatial variation of τ_a was further investigated by use of measurements made with handheld two-band Sun photometers with light-emitting diode (LED) detectors [Mims, 1999]. The wavelengths (λ) of these instruments were centered at 385 nm and 765 nm, and the instruments were intercalibrated against a CIMEL Sun photometer in Mongu on August 23, 1997. Several of these instruments were distributed at sites along the Zambezi River floodplain, with locations ranging from a site at Zambezi which was 189 km north of Mongu to Sesheke, Zambia, which was 245 km south of Mongu. At many of the sites a school teacher, missionary, or other local official was responsible for taking measurements at 30 min intervals with these instruments. We estimated the aerosol optical depth at 500 nm from these two-band instrument measurements from linear interpolation of $\ln \tau_a$ versus $\ln \lambda$. To assess the accuracy of the measurements, we made comparisons of τ_a estimated at 500 nm from the two-bands with CIMEL measurements at 500 nm. The results of these comparisons are shown in Table 2, along with a comparison of two different CIMEL instruments against each other. The root-mean-square (rms) differences of the handheld τ_{a500} values versus the CIMEL measurements at three different sites ranged from 0.045 at Mongu to 0.097 at Zambezi, while the rms difference of two CIMELS co-located in Mongu from August 29 to September 6, 1997 was 0.010.

TOMS Aerosol Index and NMC 700mb streamline

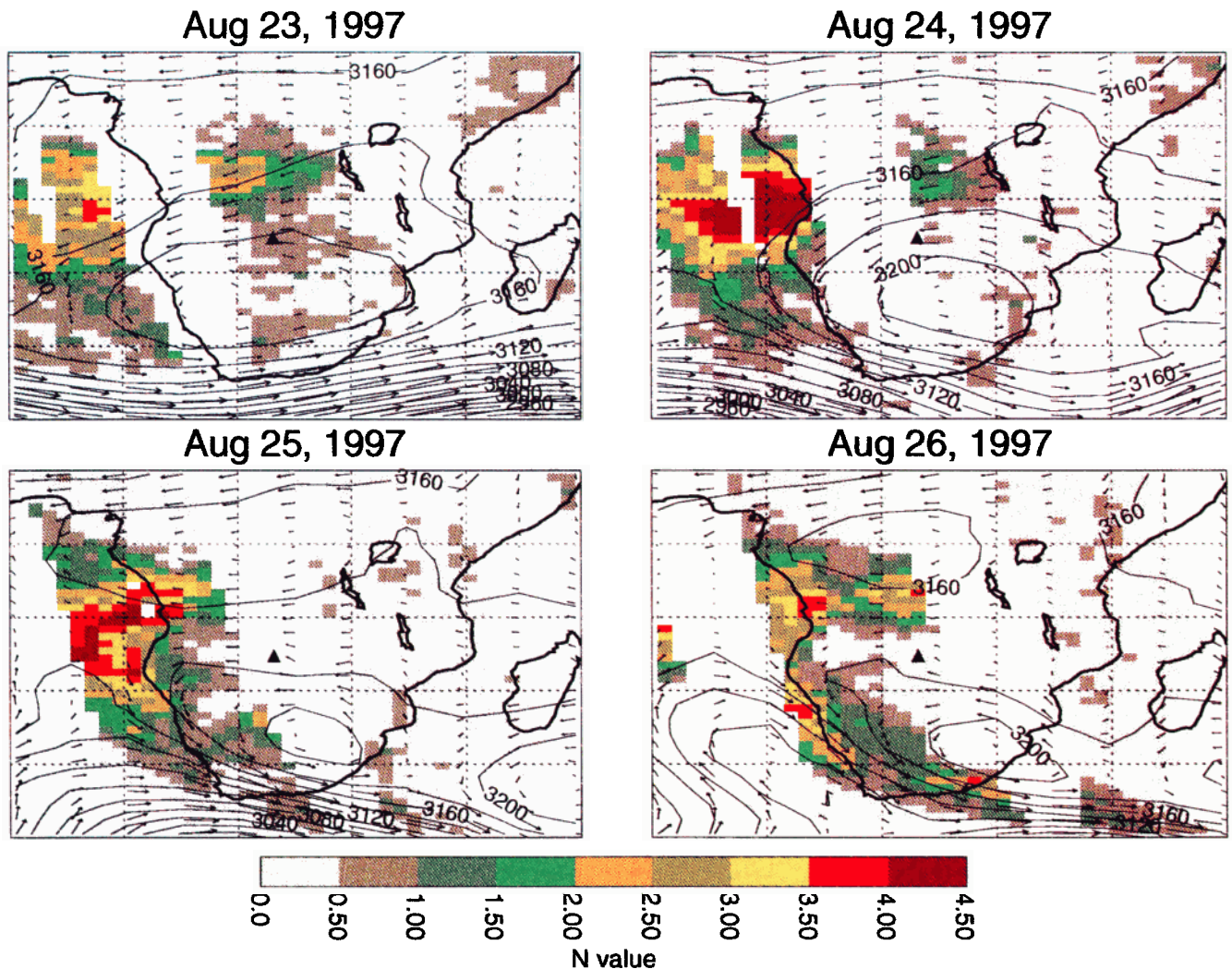


Plate 1. Earth Probe TOMS-derived aerosol index and National Meteorological Center 700 mbar streamline analysis for southern Africa for August 23–26, 1997. The black triangle near the center of each panel is the location of Mongu, Zambia. The values of geopotential height in meters at 700 mbar and the wind vectors at that level are also shown. The white areas on the maps represent data gaps between TOMS orbits.

TOMS Aerosol Index and NMC 700mb streamline

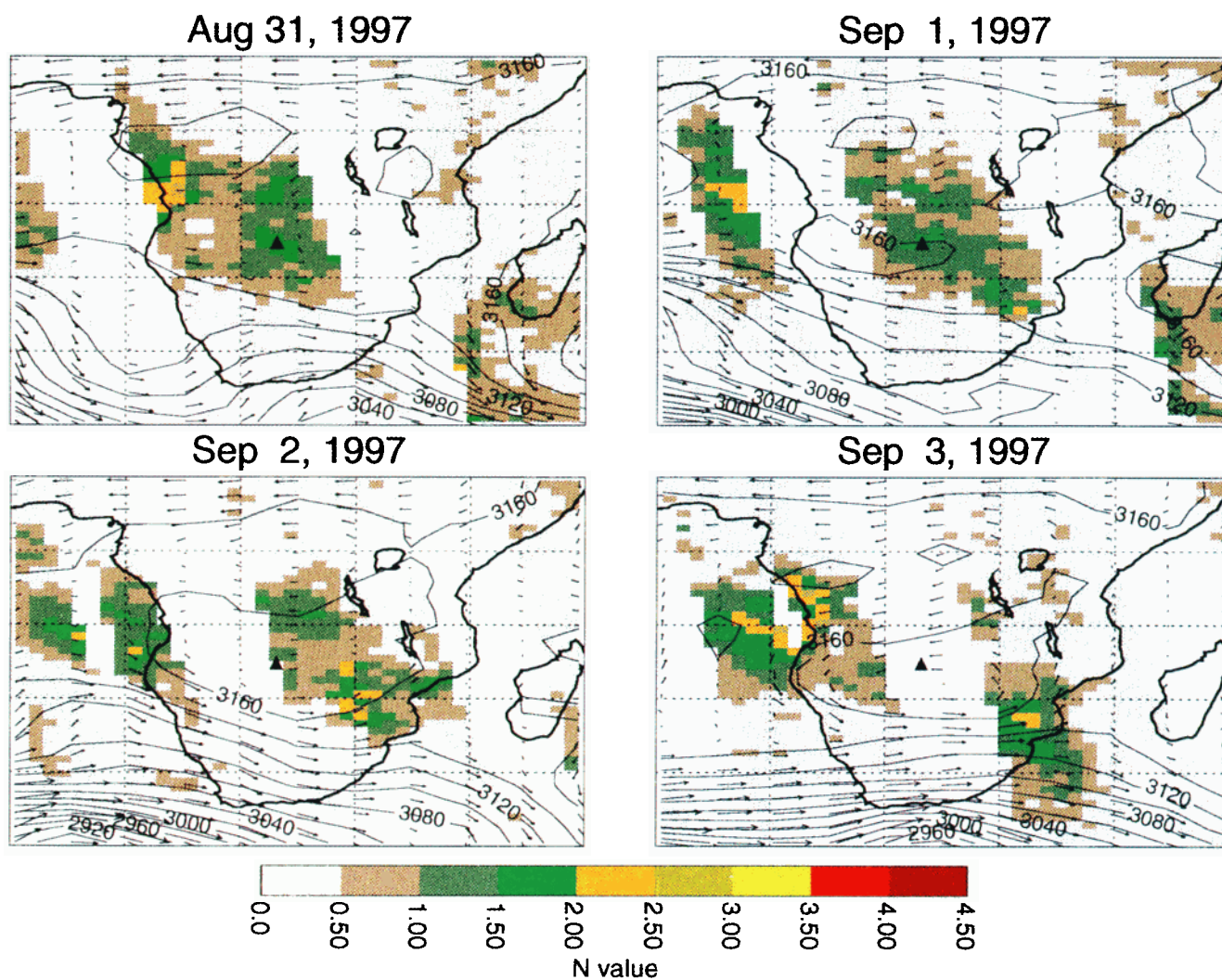


Plate 2. Same as Plate 1, but for August 31 to September 3, 1997. Note the much higher values of TOMS aerosol index over Mongu for these days compared to August 23–26, 1997 in Plate 1.

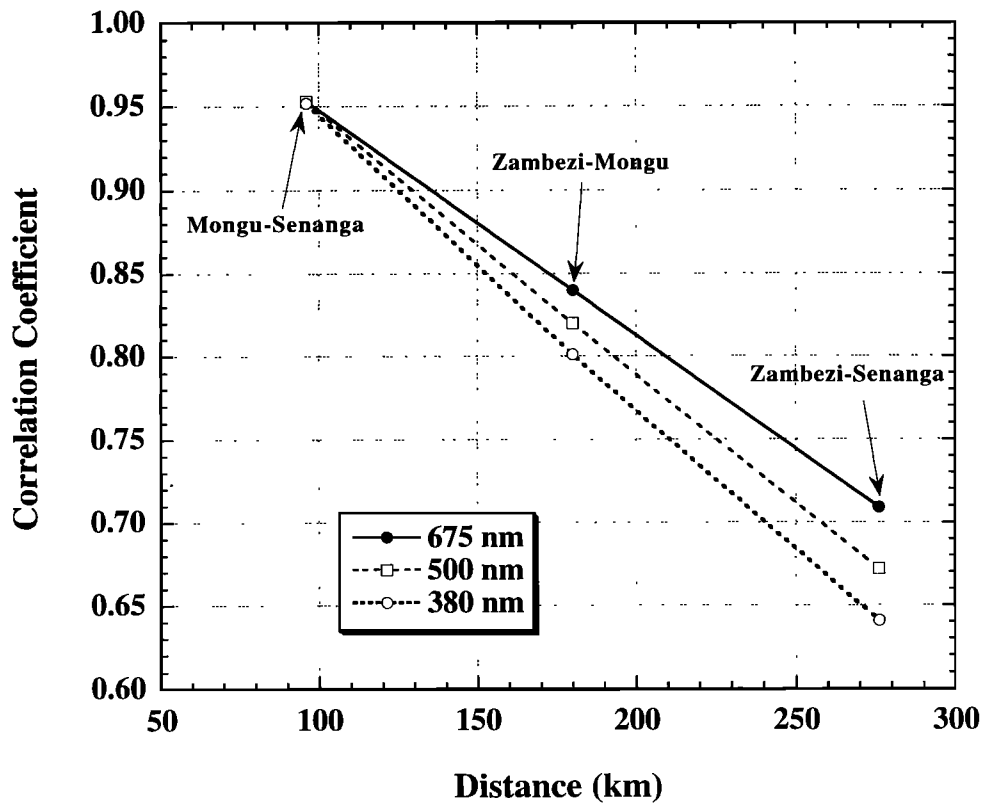


Figure 3. Correlation coefficient versus between station distance of time matched (< 3 min difference) aerosol optical depth measurements at three wavelengths (380, 500, and 675 nm) for the same three stations and time period given in Figure 2.

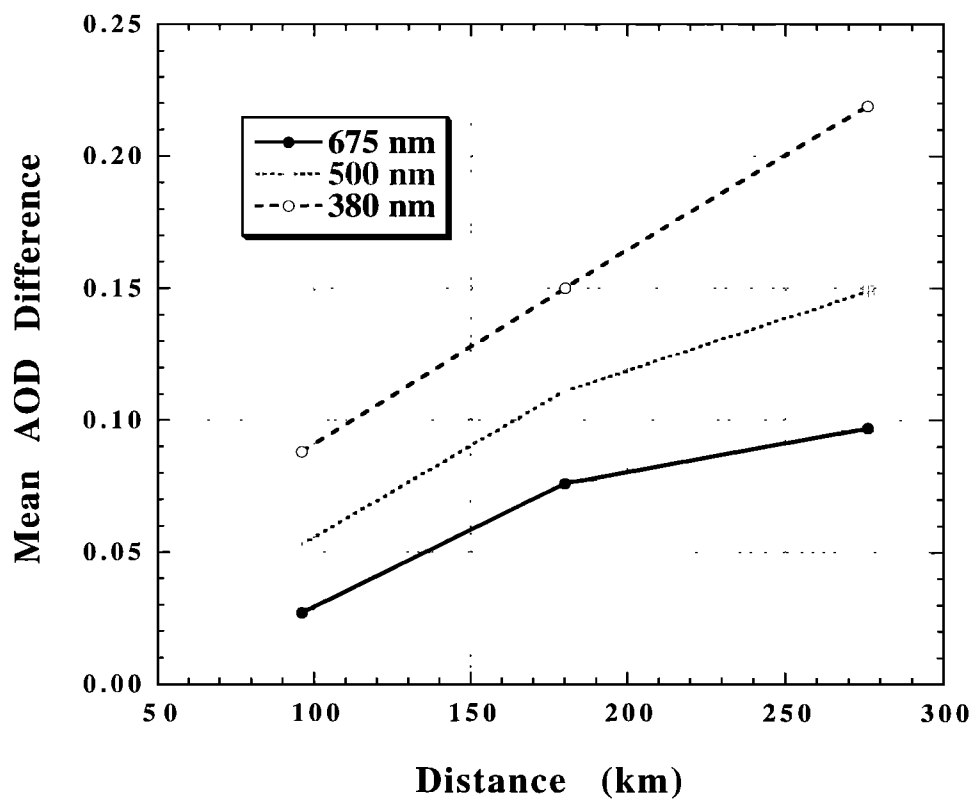


Figure 4. Mean aerosol optical depth difference (for 380, 500, and 675 nm) between stations as a function of distance between stations for the same three stations and time period given in Figure 2.

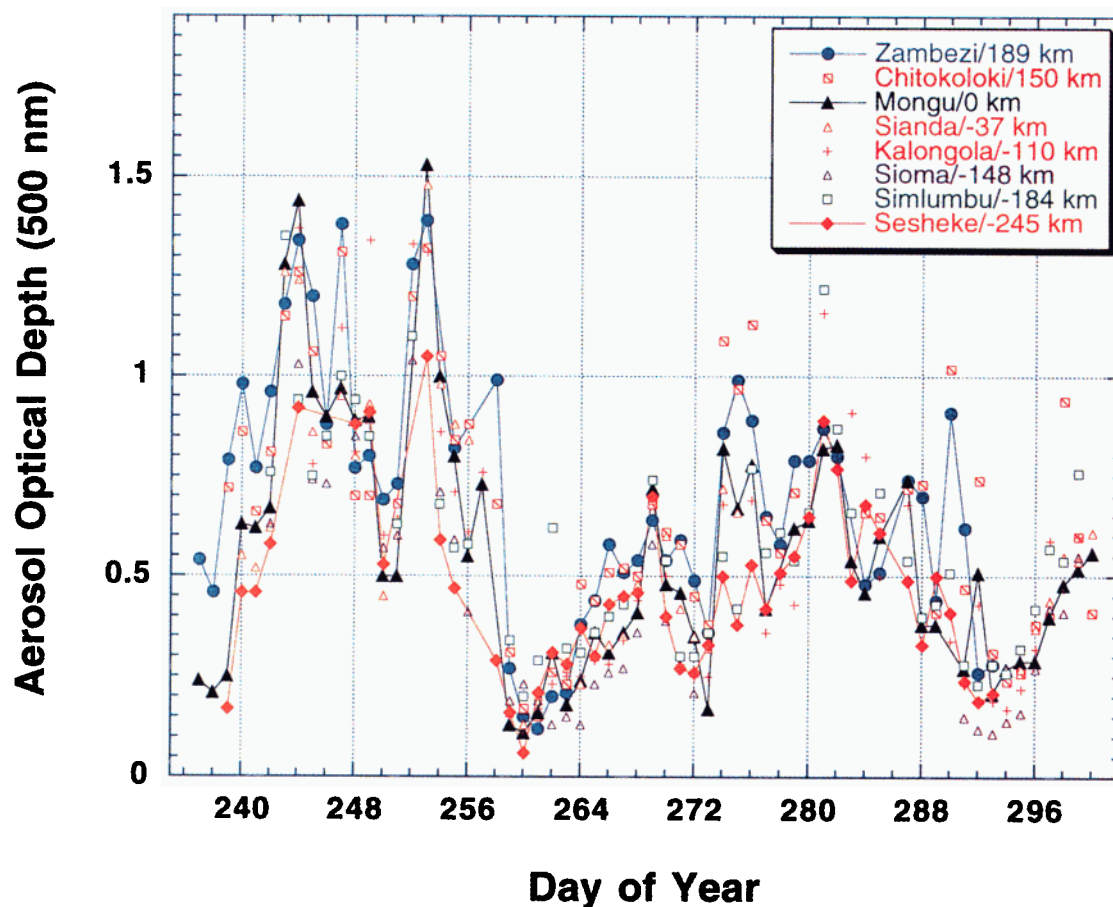


Plate 3. Time series of aerosol optical depth at 500 nm from August 25 to October 27, 1997, for eight stations located in western Zambia along a nearly north-south transect following the Zambezi River and its floodplain. The data for Mongu and Zambezi are from CIMEL automatic Sun-sky radiometers, while the data for the other six sites were obtained from handheld two-channel LED detector Sun photometers.

Table 2. Comparison of Measured Aerosol Optical Depth for Simultaneous Measurements With Different Sun Photometers

Location and Instruments	Regression Equation	r^2	RMS Difference
Mongu, Zambia CIMEL 32 versus CIMEL 12	$Y = 0.9963X + 0.00617$	0.999	0.010
Mongu, Zambia CIMEL 12 versus Handheld	$Y = 0.9851X - 0.01599$	0.987	0.045
Zambezi, Zambia CIMEL 13 versus Handheld	$Y = 0.8329X - 0.02953$	0.923	0.097
Sesheke, Zambia CIMEL 32 versus Handheld	$Y = 0.9494X - 0.02358$	0.933	0.077

Although the differences are rather large for the two-band instruments they are reasonably small compared to typical biomass burning optical depths in the burning season months. A time series (August 25 to October 27, 1997) of the handheld Sun photometer τ_{a500} data combined with the CIMEL measurements in Mongu and Zambezi, are shown in Plate 3. As was noted previously in the analysis of the spatial variance from the CIMEL data alone, there is a north-south gradient evident, with the highest values often at the northernmost site of Zambezi and the lowest values in the southernmost site of Sesheke. The low values at Sioma for the days with lowest aerosol loading, which are lower than any other site, may be due to a bias in calibration of the order of ~ 0.05 – 0.10 . The scattered high values at Chitokoloki and Simlumbu from days 274 to 300 may have been due to cloud contamination or perhaps due to local smoke plumes. The large drop in τ_{a500} after day 255 at all sites was due in part to rain, resulting in some removal of smoke aerosols and in suppression of local burning for some time, and with a subsequent steady increase of smoke after that.

4. Aerosol Physical and Radiative Properties

In addition to the magnitude and spectral variation of τ_a , two other aerosol physical/radiative properties are of prime importance in their characterization, the aerosol size distribution and single-scattering albedo. These parameters are key to the accurate computation of the radiative effects of aerosols on climate since they determine how much radiation is backscattered to space (cooling both the surface and the atmosphere) and how much is absorbed by the aerosol layer (heating the atmospheric column).

4.1. Aerosol Size Distributions

The retrieved aerosol volume size distributions for biomass burning aerosols in Mongu from August 25 to September 7, 1997 are shown in Figure 5. These size distributions were derived from the algorithm of Dubovik *et al.* [2000], which utilized measurements of spectral τ_a and almucantar sky radiance distributions (for observations when solar zenith angle $> 54^\circ$) from a CIMEL Sun-sky radiometer. These aerosol

size distributions are effective total atmospheric column-integrated size distributions that are consistent with the column-integrated radiative effects of the aerosols. As is seen in Figure 5, the accumulation mode particles ($< 0.5 \mu\text{m}$) which are nearly lognormally distributed dominate the size distribution especially at high levels of aerosol optical depth. Lognormal distributions are often utilized to parameterize the accumulation mode volume size distributions of biomass burning aerosols [Remer *et al.*, 1998; Reid *et al.*, 1998a]. It is noted that there is a tendency for increasing particle size as aerosol optical depth increases (Figure 5), with the peak in the distribution of the accumulation mode volume radius of the Mongu smoke aerosol increasing from $\sim 0.12 \mu\text{m}$ at $\tau_{a440} = 0.25$ to $\sim 0.165 \mu\text{m}$ at $\tau_{a440} = 1.40$. This increase in particle size may be related to aging of the aerosol and associated changes in size distribution as a result of coagulation, condensation, and gas-to-particle conversion [Reid *et al.*, 1998]. Even though the humidification factors (ratio of light-scattering coefficient at 80% RH to that at an RH of 30%) for biomass burning aerosol regional hazes in Amazonia was found to be relatively small (Amazonia average of 1.16 but ranging from 1.07 to 1.32 for regional averages; [Kotchenruther and Hobbs, 1998]), some of the particle growth may be the result of absorption of water vapor, especially since τ_a and PWV were highly correlated (Figure 1). However, this is very uncertain, since there is no direct relationship between PWV and RH, and it is not known whether the RH reaches sufficiently high levels in order for aerosol growth to occur from humidification.

Reid *et al.* [1998a] measured the accumulation mode size distributions of smoke in Amazonia in situ from aircraft and found that the volume median diameter varied from $0.13 \mu\text{m}$ radius for young smoke to $0.175 \mu\text{m}$ radius for aged smoke, as parameterized by lognormal size distributions. Remer *et al.*'s [1998] analysis of CIMEL almucantar data from AERONET instruments in Amazonian smoke hazes yielded accumulation mode radius values averaging $0.132 \mu\text{m}$ for savanna sites and $0.145 \mu\text{m}$ for tropical forest ecosystem sites. These values of accumulation mode lognormal volume radius for Amazonian smoke from both in situ and remote sensing techniques are similar in magnitude to accumulation mode sizes inferred from remote sensing CIMEL measurements of Zambian smoke. The coarse mode particles in Zambia also showed a tendency to increase in volume as τ_a increased, however not nearly to the magnitude of increase observed for the accumulation mode and not so strongly correlated to τ_a . It is also noted that there is a grouping of size distribution retrievals, at $\tau_{a440} = 1.05$, 1.11 , and 1.25 , where the volume distribution of the coarse mode is somewhat higher and the coarse particles smaller than for the rest of the retrievals.

In order to directly compare the size distributions inferred from the same instruments and techniques, for smoke in Amazonia to Zambian smoke, we show volume size distributions derived from inversions of AERONET measurements made in Concepcion, Bolivia (August 1998), which is located in the Amazon Basin. In Figure 6 the volume size distributions of the Mongu and Concepcion sites are compared for measurements made at equal τ_{a440} values of 0.68 . In addition, the size distribution of an urban/industrial pollution aerosol derived from data acquired at the Goddard Space Flight Center in Maryland is also shown for the same value of τ_{a440} . The size distributions shown in Figure 6 for Mongu and Concepcion are averages computed from four

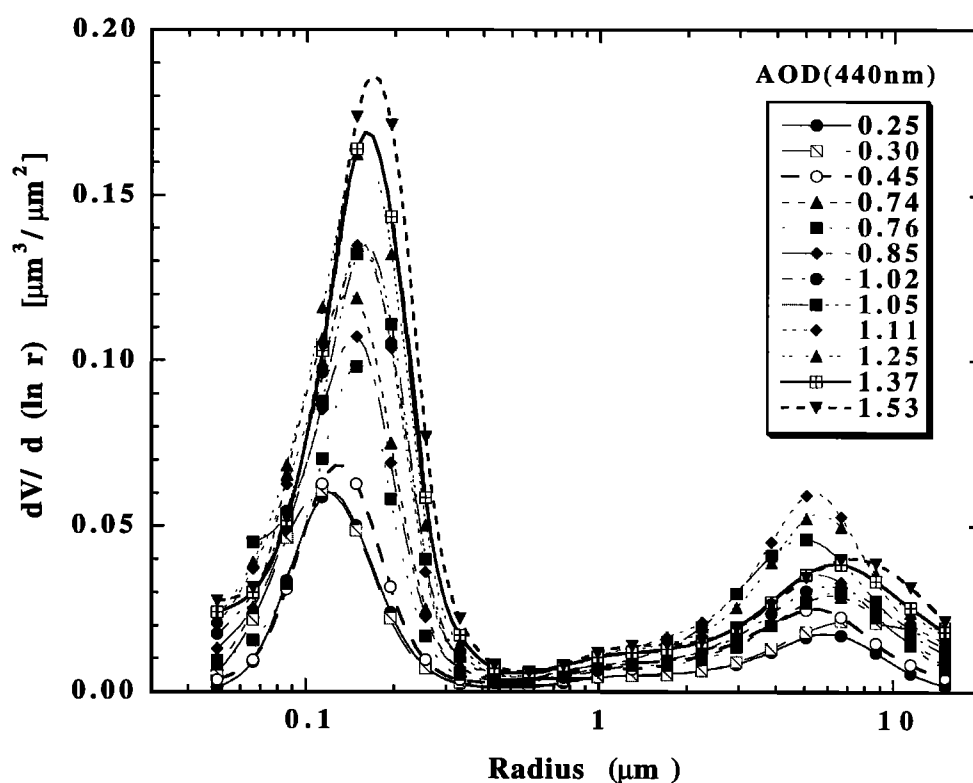


Figure 5. Aerosol volume size distributions for biomass burning aerosols in Mongu, Zambia, for August 25 to September 7, 1997, for aerosol optical depth at 440 nm varying from 0.25 to 1.53. Aerosol size distribution retrievals were derived from simultaneous analysis of sky radiances in the almucantar and spectral τ_a at 440, 675, 870, and 1020 nm.

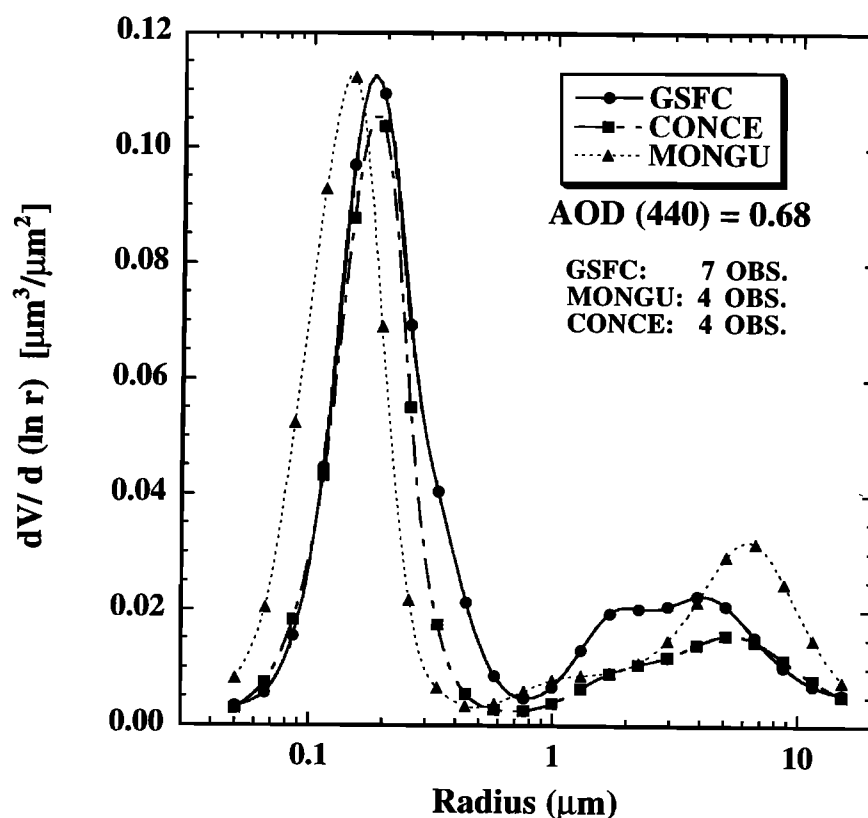


Figure 6. Comparison of aerosol volume size distribution retrievals made with AERONET radiometers at three sites, for τ_a at 440 nm of 0.68. The sites are Mongu, Zambia, with savanna burning smoke, Concepcion, Bolivia, with pasture/forest burning smoke in Amazonia, and Goddard Space Flight Center, Maryland, with urban/industrial pollution.

almucantar observation sets, while the GSFC data represent averages of seven almucantars. A shift to smaller-size accumulation mode particles is apparent for the Zambian biomass burning smoke relative to the Bolivian smoke and the U.S. mid-Atlantic pollution. The smaller size of the fine mode particles in Zambian smoke ($\sim 0.145 \mu\text{m}$) versus Bolivian smoke ($\sim 0.18 \mu\text{m}$) at this aerosol optical depth may be due to differences in the mode of combustion, the characteristics of the biomass fuel, the degree of aging of the particles, and environmental conditions such as the ambient temperature, relative humidity, fire intensity, and altitude. The biomass fuel which is burned in Zambia and surrounding countries is largely savanna grasses which often burn rapidly in flaming phase combustion, while the biomass fuel burned in Bolivia and neighboring Brazil is a combination of grass in savanna/pastures and trees from forest clearing. The woody material of varying sizes, density, and fuel moisture often burns in both flaming and smoldering phase combustion, with the smoldering phase often continuing for a much longer time period after the flaming subsides. The fuels in south central Africa are also likely to have lower moisture content than in Amazonia due to the longer more severe dry season and since the moisture content of large woody debris from forest clearing is greater than for dry grass [Guild *et al.*, 1998]. Reid and Hobbs [1998] measured the size distributions of fresh smoke (<4 min old) in Amazonia and found that the volume median diameter was greater for smoldering phase combustion ($0.145 \mu\text{m}$ radius) than for flaming phase ($0.12 \mu\text{m}$) in forested burning regions. Thus the larger-size particles in Amazonian smoke may be partly a result of a greater proportion of smoldering combustion in this environment. Another factor to consider in the size difference is the distance and speed of transport and the resultant aging of the aerosol that may have differed for these sites. Additionally, since the τ_a are equal ($\tau_{a440} = 0.68$) for all the size distribution retrievals presented in Figure 6, and since τ_a is the sum of scattering optical depth τ_{scat} and absorption optical depth τ_{abs} , differences in aerosol absorption (and therefore single-scattering albedo) will result in differences in scattering optical depth. Therefore it is expected that there would be a change in either the amplitude of the size distribution or a shift in accumulation particle size as a result of a difference in scattering optical depth. The spectral single-scattering albedo for these three sites will be compared in subsection 4.2.

The larger size accumulation mode particles for the urban/industrial pollution at GSFC are likely due to particle growth at high relative humidity and possible aerosol interactions with clouds. Kotchenruther *et al.* [1999] found that the aerosols in this mid-Atlantic coast region were very hygroscopic, with humidification factors averaging as high as 2.30 for westerly flow, as compared to an average of 1.16 for Amazonian smoke. Smirnov *et al.* [2000b] showed that for mid-Atlantic regional sites (including GSFC), the τ_{a500} increased exponentially as total atmospheric water vapor content increased (76% of the variance explained). This correlation between τ_{a500} and water vapor was attributed to aerosol and PWV transport and aerosol hygroscopicity. Remer and Kaufman [1998] found from an analysis of AERONET GSFC almucantar data that the mean radius (volume size distribution) of the accumulation mode aerosols increased roughly linearly as aerosol optical depth increased (59% of the variance explained), more than doubling, from $\sim 0.10 \mu\text{m}$ at

$\tau_{a670} \sim 0.05$ to $\sim 0.25 \mu\text{m}$ at $\tau_{a670} \sim 0.65$ (corresponding to a τ_{a440} range of ~ 0.09 to ~ 1.25).

4.2. Aerosol Single-Scattering Albedo

The single-scattering albedo ω_0 of biomass burning aerosols has a large influence on the attenuation of solar radiation and thereby diminishes irradiance incident at the Earth's surface, as a result of solar radiation absorption within the aerosol layer [Lenoble, 1991; Eck *et al.*, 1998; Christopher *et al.*, 2000]. The magnitude of ω_0 also has a large influence on the top of atmosphere (TOA) albedo and reflection function [Reid *et al.*, 1999, King *et al.*, 1999], which can result in either increases or decreases in TOA albedo as aerosol loading increases, depending on whether the Earth surface reflectance is low or relatively high. In addition, the absorption of solar radiation by smoke aerosols in the atmosphere warms the aerosol layer, which in conjunction with reduced irradiance at the surface may result in reductions in cloud cover, which Hansen *et al.* [1997] termed the "semidirect" aerosol radiative forcing effect. Since ω_0 is not expected to be well characterized from planned satellite remote sensing sensors [Kaufman *et al.*, 1997], ground-based remote sensing and in situ techniques of ω_0 estimation will continue to be very important in assessing the radiative effects of atmospheric aerosols.

Simultaneous measurements of irradiance under cloudless conditions with co-located spectral aerosol optical depth data in conjunction with the use of irradiance models allows the estimation of aerosol ω_0 . Since irradiance attenuation by atmospheric aerosols is determined primarily by spectral τ_a and ω_0 [Lenoble, 1991], irradiance models may be utilized with observations of spectral τ_a as input (using an assumed size distribution), and ω_0 estimated by varying its magnitude until measured and modeled irradiance are in agreement. This technique of ω_0 retrieval relies on the high sensitivity of the magnitude of irradiance to aerosol absorption under moderate to high aerosol loading. Details of this technique and its application to the retrieval of ω_0 for smoke aerosols over Amazonia are given by Eck *et al.* [1998]. Retrievals of ω_0 from this approach for biomass burning aerosols in Amazonia have been shown to agree well (within ~ 0.01 – 0.03) with in situ sampling techniques from aircraft [Reid *et al.*, 1998b].

A comparison of measured irradiances (under cloudless conditions) for the photosynthetically active radiation (PAR) spectral interval (400–700 nm), as influenced by differing aerosol optical depths and different aerosol types, is shown in Figure 7; measurements made at 1 min sampling intervals are shown for the solar zenith angle range of 33° to 50° . The difference in the calibration adjustment, which was described in section 2, between the two sensors located in Mongu and GSFC (in order to normalize all sensors to the same calibration), was only $\sim 1.75\%$ for this case. The highest irradiance values were measured at GSFC with low midsummer background aerosol loading ($\tau_{a500} = 0.08$) followed by a significantly reduced PAR flux 4 days later at the same site, when τ_{a500} ranged from 0.74 to 1.00 under very hazy conditions. The lowest PAR fluxes were measured in Mongu, Zambia, for a similar τ_a value ($\tau_{a500} = 0.84$) as the hazy day at GSFC, thus implying that the aerosol absorption is significantly greater for the biomass burning smoke in Zambia than for the urban/industrial pollution in the mid-

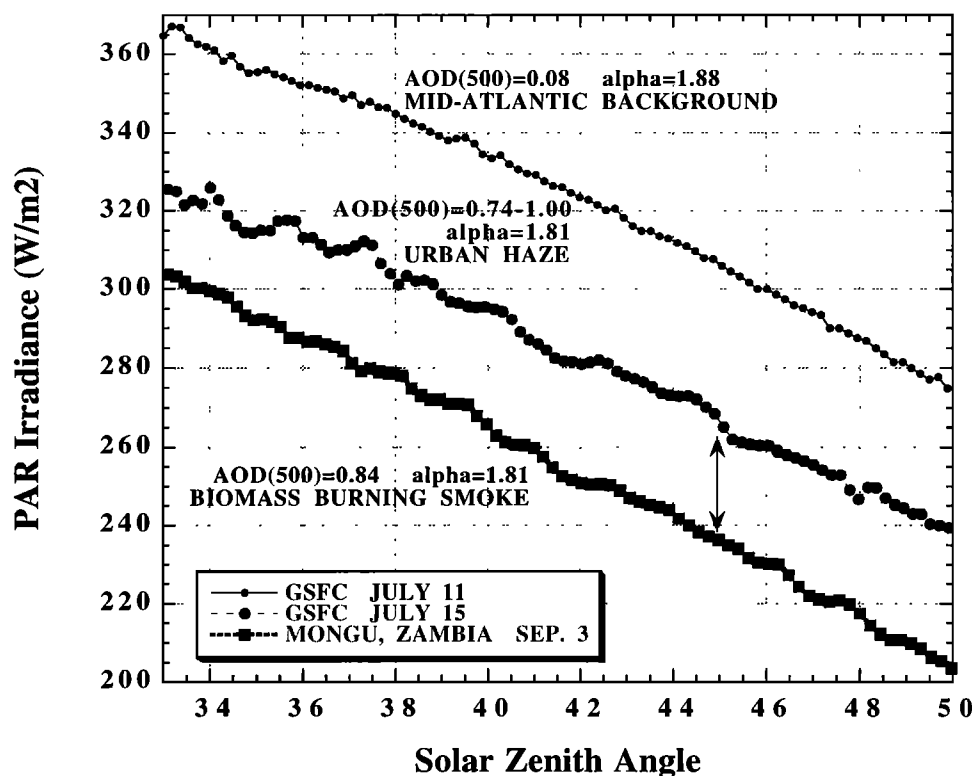


Figure 7. Measured PAR (400–700 nm) irradiance (for cloudless skies) as a function of solar zenith angle for 2 days with varying τ_a at GSFC (one clean background day and one hazy day) and one day at Mongu with a similar τ_a as for the hazy day at GSFC. Note that the Ångström wavelength exponent was similar for all 3 days. The double arrow at $\sim 45^\circ$ solar zenith shows when the aerosol optical depth at 500 nm in Mongu on September 3, 1997, and at GSFC on July 15, 1997, were nearly equal at ~ 0.84 .

Atlantic United States. It is noted that the value of the Ångström wavelength exponent (α) computed from 440 and 870 nm τ_a is very high and similar for all three cases presented in Figure 7, ranging from 1.88 to 1.81. This suggests similar size distributions dominated by accumulation mode particles (see Figure 6 and section 4.3). The sensitivity of the PAR flux to surface albedo magnitude was analyzed by varying the surface reflectance in the cloudless sky flux models, 6S and SPCTRAL2. For the levels of aerosol loading presented in the data in Figure 7, a large change in surface reflectance from values representative of vegetation to soil resulted in a 1% or less change in PAR flux at the surface, thereby suggesting that differences in surface albedo between Mongu and GSFC had a relatively small influence on the observed differences in PAR fluxes. Similarly, the model computed difference in PAR flux due to the observed differences in PWV between the sites and the dates shown in Figure 7 was only 0.2% or less.

PAR flux measurements from Mongu under cloudless sky conditions for 10 days (9 days during ZIBBEE) in 1997 were utilized to estimate ω_0 for the mid-visible (~ 550 nm). It is noted that the PAR sensor calibration adjustment described in section 2 was only 1.4% for the particular sensor located in Mongu in 1997. Therefore this adjustment resulted in differences of ~ 0.014 in ω_0 retrievals, with higher values as a result of the calibration adjustment. An example of these PAR flux measurements is shown in Figure 8, for September 3, 1997, at Mongu, when the average τ_{a500} was ~ 0.90 . SPCTRAL2 model-computed fluxes, with ω_0 assumed to be 0.80, 0.85, and

0.90, are also shown in Figure 8 for times when CIMEL τ_a measurements were available. For the SPCTRAL2 model the aerosol asymmetry factor (g) was assumed to be 0.58, the spectral reflectance for 10% green vegetation cover of Deering [1989] was assumed for the surface albedo, and spectral measured τ_a was used as input. The SPCTRAL2 model-estimated value of mid-visible ω_0 for this case was slightly higher than 0.80 for nearly the entire day. For observations made at 27° solar zenith angle on this day, the 6S model was run with two different values of the real part of the refractive index n_r (1.40 and 1.53) and with two different sources of aerosol size distribution information. The dynamic smoke aerosol model of Remer *et al.* [1998], developed from CIMEL radiometer observations made in Brazilian cerrado (savanna) regions, was utilized in addition to the size distribution retrievals of the Dubovik *et al.* [2000] algorithm for African savanna smoke in Mongu. For the 27° solar zenith angle morning observations on September 3, 1997, the 6S flux-based retrievals of ω_0 ranged from 0.809 (Remer *et al.* [1998] cerrado model with $n_r=1.40$) to 0.833 (Dubovik *et al.*, [2000] algorithm retrieval for Mongu smoke and $n_r=1.53$). This compares well with a ω_0 value of 0.804 for the SPCTRAL2 model-based retrieval. It is noted that the uncertainty in retrieved ω_0 values from the PAR flux-based technique is ~ 0.03 for $\tau_{a500} > 0.80$, due mainly to flux measurement uncertainty and to a much lesser extent, surface albedo uncertainty. For a day with very low aerosol loading ($\tau_{a500}=0.08$) in Mongu, September 17, 1997, the model-computed fluxes agreed with the measured PAR fluxes

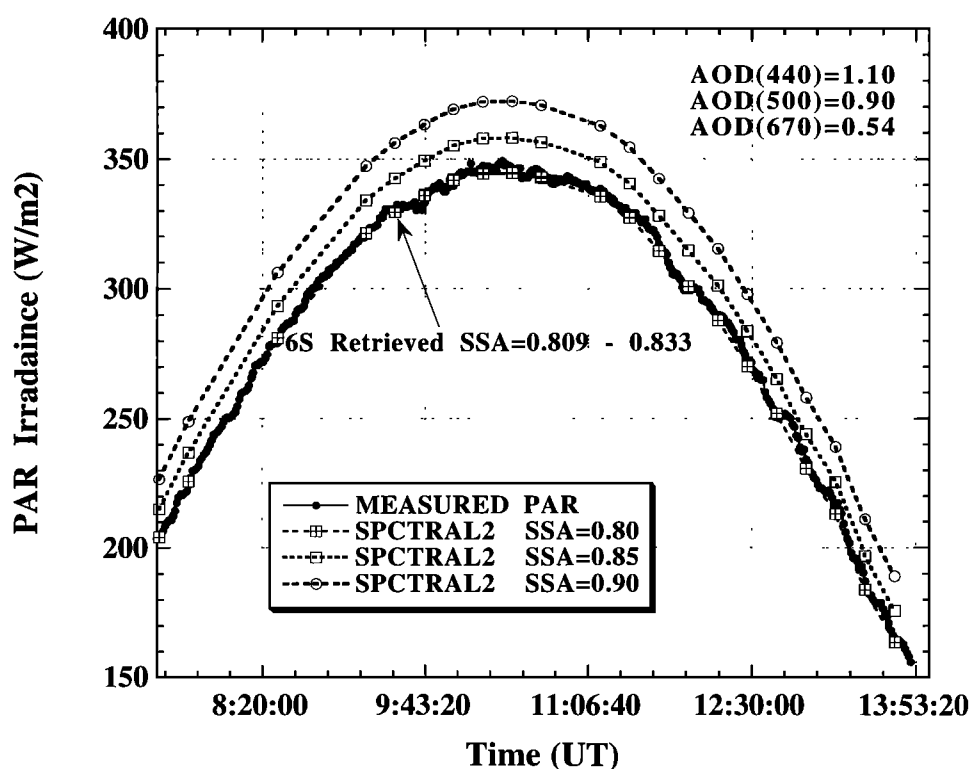


Figure 8. Measured PAR (400–700 nm) irradiance on September 3, 1997 (average $\tau_{a,500}=0.90$) in Mongu, Zambia, compared to SPCTRAL2 model calculations of PAR irradiance for different assumed values of aerosol single-scattering albedo. The SPCTRAL2 model calculations suggest that single-scattering albedo is relatively constant throughout the day at ~ 0.80 . Also shown is the retrieved ω_0 values from the 6S model at 27° solar zenith angle, ranging from 0.809 to 0.833 due to variation in the assumed size distributions and real part of the refractive index utilized (see text).

within $<1\%$ with an ω_0 value of 0.85. Table 3 shows the 6S model-based estimates of ω_0 for the various combinations of size distributions and refractive index and also the SPCTRAL2 model-based retrievals. Differences in the 6S ω_0 retrievals due to differences in the assumed size distributions range from 0.0 to 0.02, with the retrievals made with the *Remer et al.* [1998] aerosol model having lower ω_0 values, due partly to these size distributions having both a broader accumulation mode and a larger coarse mode and thus greater forward scattering of solar radiation. The mean of all 10 retrieved ω_0 values (for 10 days) in Table 3 ranged from 0.815 for the SPCTRAL2 model retrievals, to 0.827 for the 6S model retrievals with $n_r=1.53$ and the *Remer et al.* [1998] cerrado model, to 0.838 for the 6S model retrievals with the *Dubovik et al.* [2000] size distributions for Mongu smoke and $n_r=1.53$.

Retrievals of ω_0 made by applying the algorithm of *Dubovik et al.* [2000] to the CIMEL-measured spectral sky radiances in the almucantar and τ_a from direct Sun measurements were compared to the PAR flux-based retrievals (Figure 9). All of these retrievals were made in western Zambia during the ZIBBEE experiment, from August 28 to September 12, 1997. The ω_0 values shown in Figure 9 are estimates for 550 nm, computed from an averaging of the 440 nm and 675 nm retrievals from the *Dubovik et al.* algorithm and also from ω_0 inferred from broadband PAR (400–700 nm) flux measurements. The retrievals were made on different days, in some cases when stations in different locations were compared (Mongu, Senanga, and Zambezi). For retrievals made in the

same location (Mongu) the observations were often from different times on the same days, depending on the availability of data and also on the algorithm requirements (solar zenith angle limits) for the different retrieval techniques. The repeatability of retrievals using this technique and AERONET CIMEL radiometers was demonstrated for the Mongu site where the *Dubovik et al.* algorithm yielded similar results (ω_0 differences <0.01 on average) when applied to the data of two different instruments. The retrievals of ω_0 for Zambezi were very similar in magnitude to that of the Mongu sites (average difference <0.01) and for Senanga were 0.01–0.02 higher than the averages for the two Mongu sites. These results suggest that the absorption properties of the biomass burning smoke were similar throughout western Zambia and that ω_0 was relatively constant as a function of aerosol optical depth. For the PAR flux-based retrievals of ω_0 , based on application of the *Dubovik* size distributions, two different size distributions were used, one retrieved when $\tau_{a,440}=0.80$ which was applied to cases when $\tau_{a,440}$ ranged from 0.7 to 1.1 and one for $\tau_{a,440}=1.6$ when $\tau_{a,440}$ ranged from 1.5 to 1.8. The PAR flux-based retrievals of ω_0 in Figure 9 are averages of retrievals made with the two different assumed values of the real refractive index, 1.40 and 1.53. The average of the ω_0 retrievals, shown in Figure 9 which were made with the *Dubovik et al.* algorithm and CIMEL data alone for Mongu for this time period was 0.851 for one instrument and 0.860 for another. The average retrieved ω_0 from the PAR flux/6S model retrieval was 0.836 when the *Dubovik* size distributions were

Table 3. Retrievals of Single-Scattering Albedo (ω_0) From PAR Irradiance Measurements Utilizing the 6S and SPCTRAL2 Models. Showing the Influence of Aerosol Size Distribution and the Real Refractive Index n_r for 6S

1997 (Mongu)	Solar Zenith Angle	τ_{500}	$\alpha_{(500/670)}$	6S – Dubovik		6S – Remer		SPCTRAL2 ω_0
				ω_0	n_r	ω_0	n_r	
Aug. 28	27.2°	0.56	1.76	0.837	1.53	0.825	1.53	0.840
				0.836	1.40	0.815	1.40	
Aug. 29 (Litoya)	24.9°	0.58	1.79	0.813	1.53	0.800	1.53	0.811
				0.805	1.40	0.789	1.40	
Aug. 30	28.3°	0.68	1.77	0.829	1.53	0.815	1.53	0.819
				0.824	1.40	0.804	1.40	
Aug. 31	32.5°	1.29	1.78	0.843	1.53	0.840	1.53	0.799
				0.834	1.40	0.830	1.40	
Sept. 1	34.9°	1.30	1.72	0.851	1.53	0.851	1.53	0.809
				0.846	1.40	0.840	1.40	
Sept. 3	27.0°	0.85	1.75	0.833	1.53	0.816	1.53	0.804
				0.830	1.40	0.809	1.40	
Sept. 4	34.1°	0.93	1.77	0.833	1.53	0.816	1.53	0.799
				0.830	1.40	0.809	1.40	
Sept. 5	43.1°	0.77	1.75	0.833	1.53	0.816	1.53	0.810
				0.830	1.40	0.809	1.40	
Sept. 10	20.1°	1.45	1.73	0.847	1.53	0.842	1.53	0.804
				0.840	1.40	0.833	1.40	
Oct. 2	13.7°	0.70	1.80	0.859	1.53	0.847	1.53	0.855
				0.856	1.40	0.833	1.40	

used and 0.822 when the Remer et al. size distributions were used. The uncertainty in ω_0 retrieval for both techniques (PAR flux/ τ_a and almucantar radiances/ τ_a) is ~ 0.03 , and therefore these estimates fall within the uncertainty range of each other.

The ω_0 retrievals made from the Dubovik et al. [2000] algorithm utilizing CIMEL sky radiance measurements and direct Sun-measured τ_a are calculated for the four sky radiance measurement wavelengths (nominal) of 440, 675, 870, and 1020 nm. A comparison of these spectral ω_0 retrievals for Mongu during ZIBBEE to values also obtained with CIMEL instruments in Concepcion, Bolivia (biomass burning, for August 1998), and GSFC (urban/industrial, June–September 1998) is given in Figure 10. The differences in the magnitude of ω_0 for biomass burning smoke in Mongu and Concepcion are significant and very large. As previously discussed (in section 4.1), the differences in combustion phase (flaming versus smoldering), fuel moisture content, and aging of the aerosol are all possible factors contributing to differences in the aerosol absorption characteristics. Because of the difference in biomass fuel type (primarily grass in Zambia and mixed pasture/ forest trees in Bolivia) it is likely that the flaming phase contributes a higher proportion of the total combustion in Zambia, thus resulting in a greater fraction of black carbon in the total aerosol [Ward et al., 1996]. Reid and Hobbs [1998] measured the absorption of fresh smoke (<4 min old) in Amazonia and found that ω_0 was greater for smoldering phase combustion (mean of 0.84 at 550 nm) than for flaming phase (mean of 0.74 at 550 nm) in forested burning regions. The slopes of ω_0 as a function of wavelength, shown in Figure 10, are similar to those inferred by Eck et al. [1998] from spectral irradiance retrievals for biomass burning aerosols in

Cuiaba, Brazil. For one case, where trajectory analysis showed that the smoke in Cuiaba originated from cerrado (savanna) burning regions, Eck et al. [1998] found a strong wavelength dependence of ω_0 . However, for another case where trajectories suggested advection of smoke from rain forest regions to the north of Cuiaba, the wavelength dependence of ω_0 was of a lesser extent and the single-scattering albedo was also higher. For comparison, the spectral retrievals of ω_0 for GSFC, which represents urban/industrial aerosol in the mid-Atlantic United States, show significantly less absorption than even the smoke in Concepcion, Bolivia, and with less wavelength dependence (Figure 10).

4.3. Wavelength Dependence of τ_a

Analysis of the spectral dependence of τ_a is important for the interpretation of remote sensing retrievals of τ_a from satellite or other platforms, when the aerosol size distribution and spectral ω_0 may not be accurately known. Many studies involving the application of aerosol optical properties information do not adequately account for the detailed spectral variation of τ_a . Knowledge of the spectral dependencies of τ_a is important in both interpolation and extrapolation of τ_a beyond measured values for use in flux and energy balance computations, and atmospheric correction of remote sensing data.

The wavelength dependence of the aerosol optical depth is dependent primarily on the aerosol size distribution and also to a much lesser extent on the absorption characteristics of the aerosol. To investigate the wavelength dependence of τ_a in Mongu over a complete burning season, we analyzed

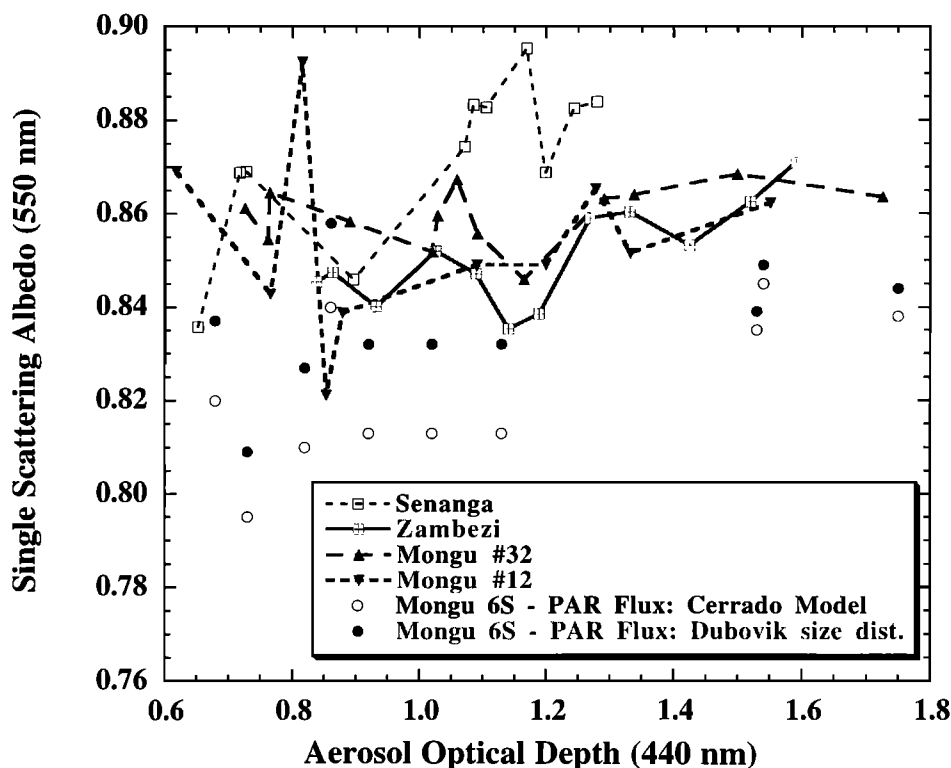


Figure 9. Comparison of ω_0 retrievals at ~ 550 nm as a function of aerosol optical depth at Mongu, Zambia, for the period August 28 to September 12, 1997. Retrievals of ω_0 from CIMEL instrument Sun and sky radiances and the algorithm of *Dubovik et al.* [2000] are shown for three sites and also for two different instruments at Mongu. These retrievals suggest that there was relatively little spatial variance of ω_0 in western Zambia and also relatively constant ω_0 values as a function of τ_{440} . Also shown are retrievals of ω_0 from the PAR flux measurements, utilizing two different assumed size distributions (see text).

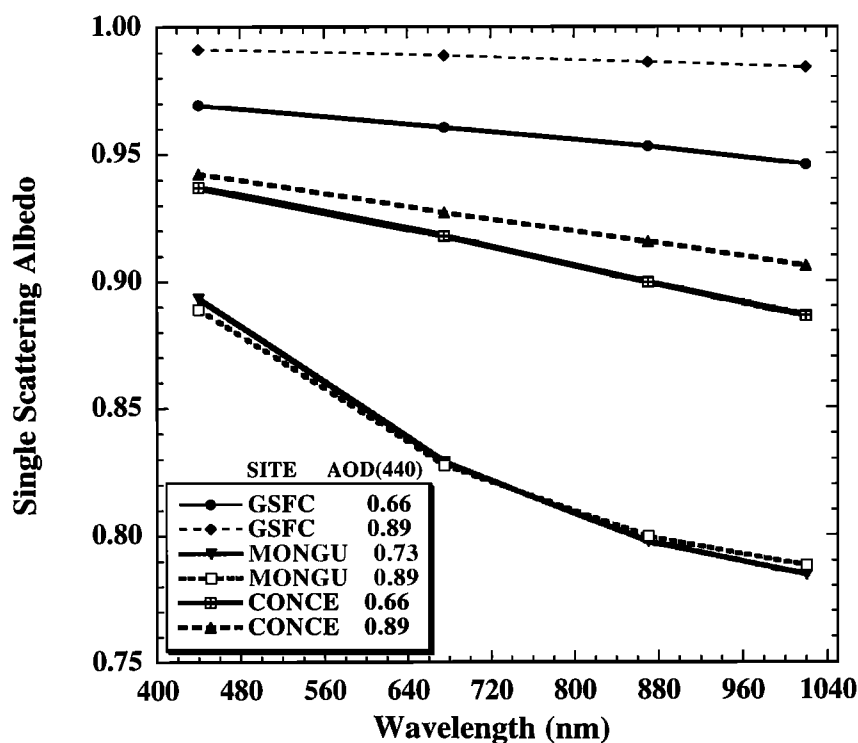


Figure 10. Comparison of spectral (440 to 1020 nm) ω_0 retrievals made with AERONET radiometers at three sites, for τ_{440} at 440 nm ranging from 0.66 to 0.89. The sites are Mongu, Zambia, with savanna burning smoke, Concepcion, Bolivia, with pasture/forest burning smoke in Amazonia, and Goddard Space Flight Center, Maryland, with urban/industrial pollution. See Figure 6 for a comparison of the aerosol volume size distribution for these same sites.

AERONET measurements made in 1998 which had more days with very high τ_a , since 1997 was an El Niño year with some early rainfall events after the first week of September. The Ångström wavelength exponent [Ångström, 1929], which quantifies the wavelength dependence of τ_a , may in the simple case of two spectral channels be computed from spectral values of τ_a using:

$$\alpha = -\frac{d \ln \tau_a}{d \ln \lambda} = -\frac{\ln\left(\frac{\tau_{a_2}}{\tau_{a_1}}\right)}{\ln\left(\frac{\lambda_2}{\lambda_1}\right)}, \quad (1)$$

and therefore α , as defined in equation (1), is the negative of the slope (or negative of the first derivative) of τ_a with wavelength in logarithmic scale. In Figure 11a the Ångström wavelength exponent (α), computed from the linear regression of individual $\ln \tau_a$ measurements versus $\ln \lambda$ for 440, 500, 675, and 870 nm, is shown as a function of aerosol optical depth at 440 nm, for July 22 through November 21, 1998, in Mongu (cloud screened by the Smirnov *et al.* [2000a] algorithm). The values of α for high aerosol optical depth ($\tau_{a440} > 0.5$) range from ~ 1.6 to 2.0, which are similar to values measured for these same wavelengths for biomass burning smoke in Amazonia [Eck *et al.*, 1999] and for smoke from boreal forest fires [Markham *et al.*, 1997]. Lioussé *et al.* [1995] found α (computed for similar wavelengths: 450, 650, and 850 nm τ_a) for savanna burning smoke to range from 0.84 for aged smoke to 1.42 for fresh smoke at Lamto, Ivory Coast. However, in that West African location it is possible that these relatively low α values may be influenced by the presence of Sahelian/Saharan coarse mode dust as a second aerosol type. For lower τ_a in Mongu ($\tau_{a440} < 0.5$) the values of α decrease as τ_a decreases due (Figure 11a) to the increasingly larger influence of the coarse mode in the aerosol size distribution (Figure 5), while at higher τ_a the accumulation mode biomass burning aerosols dominate.

The Ångström wavelength exponent computed from instantaneous τ_a measurements at 380 and 500 nm (equation (1)) is shown in Figure 11b, with seven points out of a total of 2284 not shown for $\alpha_{(380-500)} < 1.00$. As shown by Reid *et al.* [1999], from Mie calculations utilizing measured size distributions of biomass burning aerosols in Amazonia, the Ångström exponent at shorter wavelengths is more sensitive than at longer wavelengths to changes in particle size and width of the accumulation mode. Therefore the decrease of $\alpha_{(380-500)}$ with increasing aerosol optical depth (Figure 11b) is related to the increase in accumulation mode particle size as τ_a increases, which is also shown in Figure 11b. The fine mode radius size shown in Figure 11b is determined as the maximum value of $dV/d(\ln r)$ of the accumulation mode size distribution (see Figure 5). This increase in particle size with increasing aerosol optical depth is most likely due to the aging processes of coagulation, condensation, and gas-to-particle conversion [Reid *et al.*, 1998a], and also due in part to aerosol hygroscopic growth since at high aerosol optical depths, there is a correlation between PWV and τ_a (Figure 1). Reid *et al.* [1999] showed similar relationships (to those shown in Figures 11a and 11b) between both short and longer wavelength α versus τ_a for Amazonian smoke. Therefore α at longer wavelengths can be utilized to provide information on the relative influence of coarse versus accumulation mode aerosols, while α at short wavelengths is much more sensitive

to the size of the accumulation mode aerosols with much less influence of the coarse mode for biomass burning aerosols (see also O'Neill *et al.* [2000]).

A second-order polynomial fit to the $\ln \tau_a$ versus $\ln \lambda$ data provides excellent agreement with measured τ_a resulting in differences of the order of the uncertainty in the measurements (~ 0.01 – 0.02), while a linear fit of $\ln \tau_a$ versus $\ln \lambda$ (α) yields significant differences with measured τ_a . For example, in Mongu on September 1, 1997, at 0858 UT when $\tau_{a500} = 1.29$, the linear fit of $\ln \tau_a$ versus $\ln \lambda$ for seven wavelengths from 340 to 1020 nm resulted in an overestimate of τ_a by 0.26 at 340 nm and an underestimate at 500 nm by 0.11. The second-order fit for this case resulted in agreement with measured τ_a values of 0.03 or less. As a parameter to quantify the curvature of the $\ln \tau_a$ versus $\ln \lambda$ relationship we utilize the second derivative of $\ln \tau_a$ versus $\ln \lambda$, or the derivative of α with respect to the logarithm of wavelength [Eck *et al.*, 1999]. The second derivative is a measure of the rate of change of the slope with respect to wavelength and therefore is a complement to the Ångström exponent, which is the negative of the slope (first derivative) of $\ln \tau_a$ versus $\ln \lambda$. We use the following approximation to compute the second derivative [Li *et al.*, 1993], and we define $\alpha'(\lambda_i)$ at wavelength λ as the negative of the second derivative (since α is defined as the negative of the first derivative):

$$\alpha'(\lambda_i) = \frac{d\alpha}{d \ln \lambda} = -\left(\frac{2}{\ln \lambda_{i+1} - \ln \lambda_{i-1}} \right) \left(\frac{\ln \tau_{a,i+1} - \ln \tau_{a,i}}{\ln \lambda_{i+1} - \ln \lambda_i} - \frac{\ln \tau_{a,i} - \ln \tau_{a,i-1}}{\ln \lambda_i - \ln \lambda_{i-1}} \right). \quad (2)$$

The values of α' for Mongu, computed from the 340, 440, and 870 nm τ_a , are shown in Figure 12a as a function of τ_{a440} for the same data set as was used in Figure 11. Large positive values of α' are characteristic of fine mode dominated aerosol size distributions [Eck *et al.*, 1999], which were also observed for biomass burning aerosols in Amazonia, while near zero and negative values of α' are characteristic of size distributions with a dominant coarse mode or bimodal distributions with a coarse mode having a significant relative magnitude [Eck *et al.*, 1999; O'Neill *et al.*, 2000]. For cases where α' is positive, a linear (Ångström) fit of $\ln \tau_a$ versus $\ln \lambda$ for all wavelengths will result in the linear fit overestimating τ_a at the lowest and highest wavelengths and underestimating τ_a at the middle wavelengths. It is noted that even though α' at low τ_a ($\tau_{a500} < 0.25$) reaches values as low as -1.40 , the departure from linearity ($\alpha' = 0$) of $\ln \tau_a$ versus $\ln \lambda$ for these cases is only ~ 0.01 to 0.02 in τ_a , which is similar to τ_a measurement uncertainty and thus not very significant. A comparison of α' for high aerosol optical depth cases only ($\tau_{a440} > 0.5$) between Mongu and GSFC data (June–September 1998) is shown in Figure 12b. It is noted that the measured α' values are significantly higher for the aerosol at GSFC than for the biomass burning aerosols at Mongu.

To further investigate the effects of aerosol absorption and particle size on the magnitude of α' , we have computed spectral extinction coefficients from Mie computations for unimodal lognormal volume size distributions with an accumulation mode only. The assumption of the lack of a coarse mode is a reasonable approximation for high aerosol optical depths since we have shown (Figure 6) that the

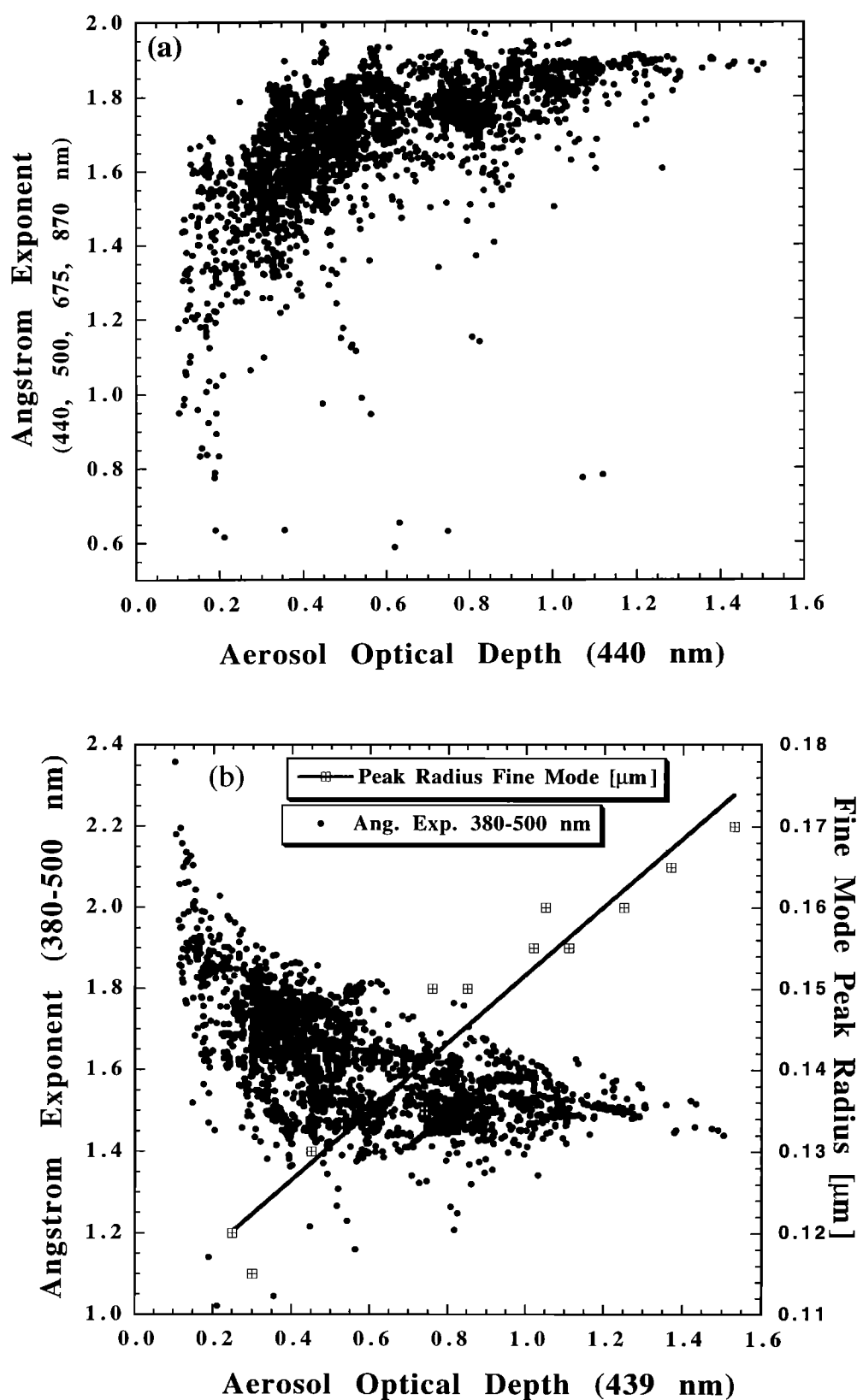


Figure 11. (a) Ångström wavelength exponent (α) computed from linear regression of $\ln \tau_a$ versus $\ln \lambda$ from instantaneous τ_a values at 440, 500, 675, and 870 nm for Mongu, Zambia for July 22 to November 21, 1998, as a function of aerosol optical depth at 440 nm. (b) The Ångström wavelength exponent computed from the 380 and 500 nm wavelength pair using equation (1), for the same data as shown in (Figure 11a). Also shown in Figure 11b is the radius of the fine mode peak value of $dV/d \ln r$ for Mongu, determined from the data shown in Figure 5.

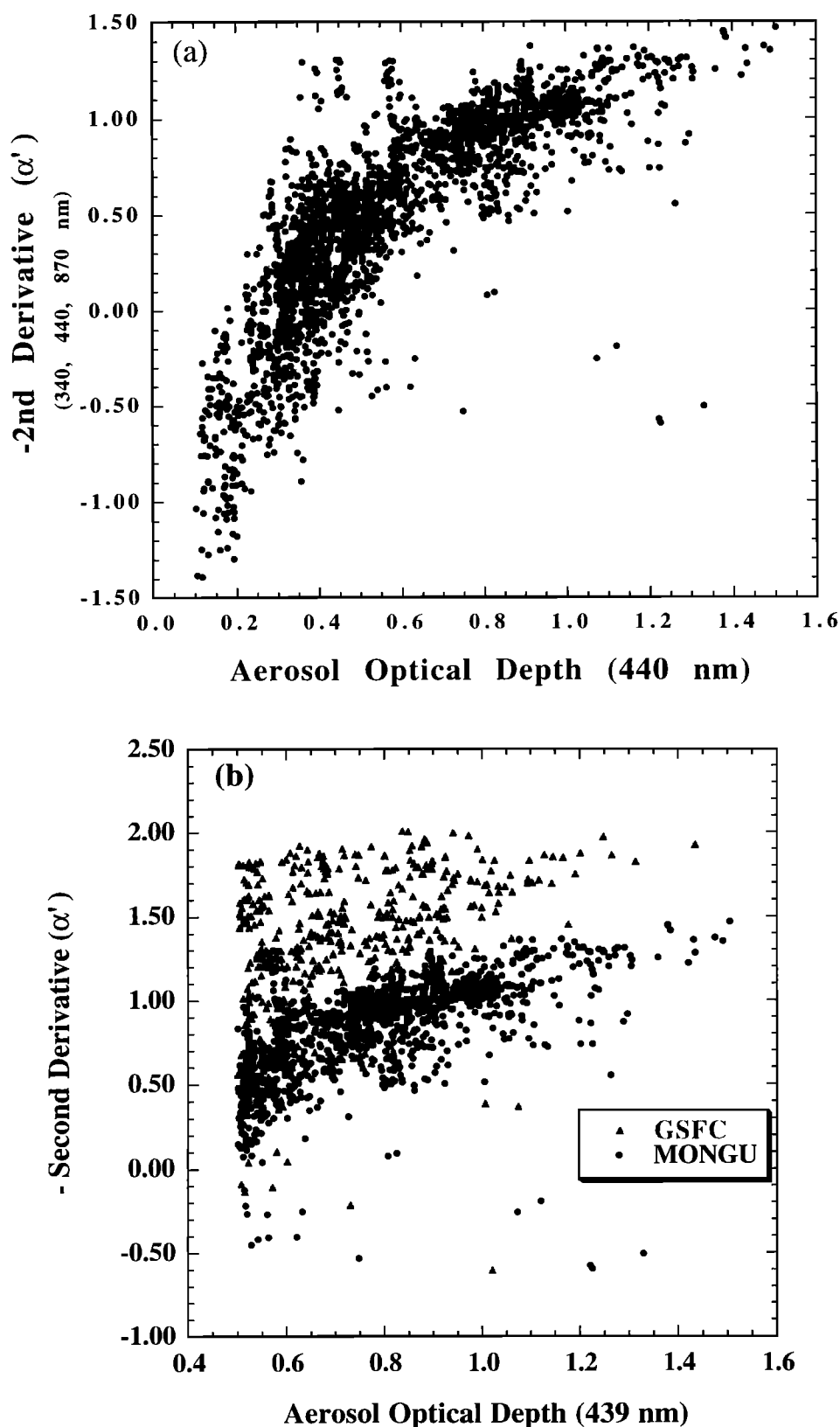


Figure 12. (a) Value of α' ($d\alpha/d \ln \lambda$) computed from instantaneous τ_a values at 340, 440, and 870 nm for Mongu, Zambia, for July 22 to November 21, 1998, as a function of aerosol optical depth at 440 nm. (b) Comparison of α' values from Mongu, Zambia, to values computed for GSFC, Maryland (June-September 1998) for $\tau_{a440} > 0.5$.

accumulation mode dominates at these τ_a levels at these sites. In Figures 13a, 13b, and 13c we present the results of these Mie computations, with extinction coefficients from 340 to 1020 nm normalized to the value at 500 nm. For the computations made with varying black carbon content (Figure 13a), the modal radius was fixed at 0.15 μm with a geometric standard deviation of the lognormal distribution of 1.50. The computations made for the variation in modal size (radius) of the particles (Figure 13b) assumed no absorption ($\omega_0=1$); the real part of the refractive index was held at 1.43, with a geometric standard deviation of the lognormal distribution of 1.50. The computations made for the variation in a geometric standard deviation of the particle size distribution (Figure 13c) also assumed no absorption ($\omega_0=1$); the real part of the refractive index was held at 1.43, with an accumulation mode radius of 0.15 μm . These figures show the sensitivity of α' to the effects of changes in black carbon content (absorption) in the aerosol, to changes in the modal size of the accumulation mode aerosols, and to changes in the geometric standard deviation of the lognormal volume size distribution. For aerosols with increasing amounts of black carbon (zero to 30%), the Mie computations show that the value of α' subsequently decreases, while for increasing size of the accumulation mode particles (0.10 to 0.30 μm radius) the value of α' increases, and for narrower lognormal size distributions

(decreasing geometric standard deviation) the value of α' increases. It is noted that the geometric standard deviations of the size distributions (from the Dubovik *et al.* [2000] retrievals) are very similar for both sites (GSFC and Mongu) for $\tau_{a440}>0.5$, ranging from 1.47 to 1.53 in Mongu to 1.48 to 1.55 at GSFC. Therefore given the sensitivity of α' to geometric standard deviation changes (Figure 13c) and its similar magnitude at both sites, we conclude that this aspect of the aerosol size distribution had relatively little influence on the differences in α' observed in Figure 12b. As was seen in our previously presented retrievals from the AERONET instrument data, the single-scattering albedo for the GSFC site was much higher than for Mongu (Figure 10) and the size of the accumulation mode aerosols was larger for GSFC than for Mongu (Figure 6). Thus the observed higher values of α' for GSFC relative to Mongu (Figure 12b) are consistent with the trends predicted by Mie theory in conjunction with the differences in aerosol absorption and particle size inferred from the retrievals. Therefore aerosols which are only weakly absorbing and/or which have relatively large-size accumulation mode particles will exhibit the largest departures from linearity of the $\ln \tau_a$ versus $\ln \lambda$ relationship. Complete knowledge of the wavelength dependence of τ_a and the factors influencing it is required for accurate extrapolation or interpolation of measured values. Applications of this

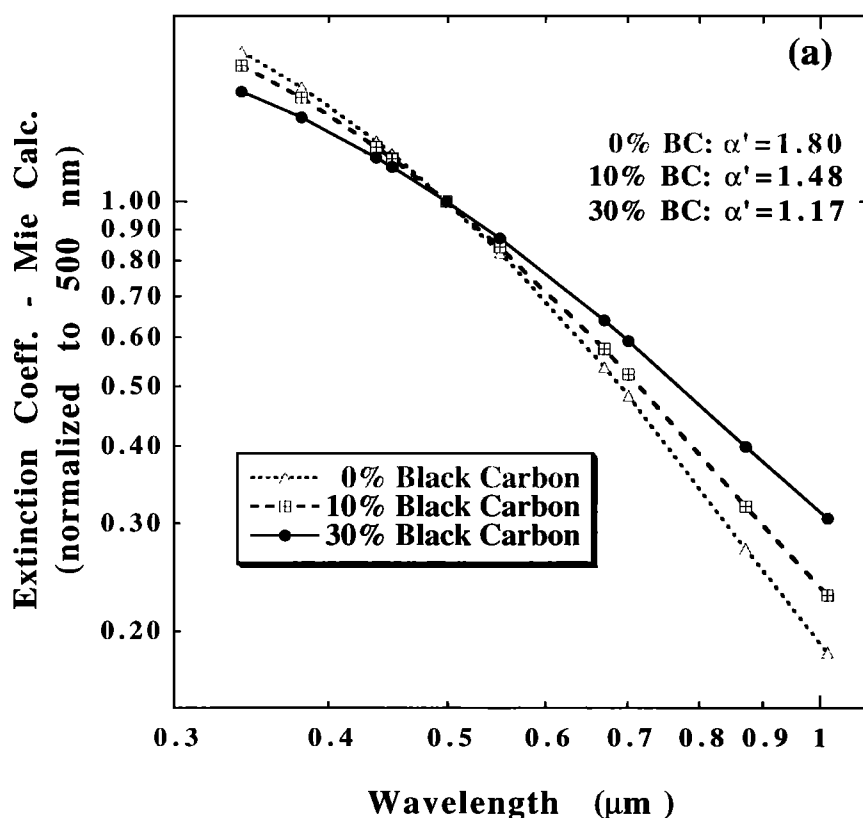


Figure 13. (a) Mie calculations of the extinction coefficient (normalized to 500 nm) versus wavelength and the resultant computed values of α' for differing amounts of black carbon (0, 10, and 30%) for an accumulation mode only lognormal size distribution with mode radius of 0.15 μm and geometric standard deviation of 1.50. (b) Same as Figure 13a but for differing values of the mode radius from 0.10 to 0.30 μm , for aerosol with no absorption ($\omega_0=1$), real refractive index fixed at 1.43, and geometric standard deviation fixed at 1.50. (c) Same as Figure 13a but for differing values of the geometric standard deviation from 1.25 to 2.00, for aerosol with no absorption ($\omega_0=1$), real refractive index fixed at 1.43, and mode radius fixed at 0.15 μm .

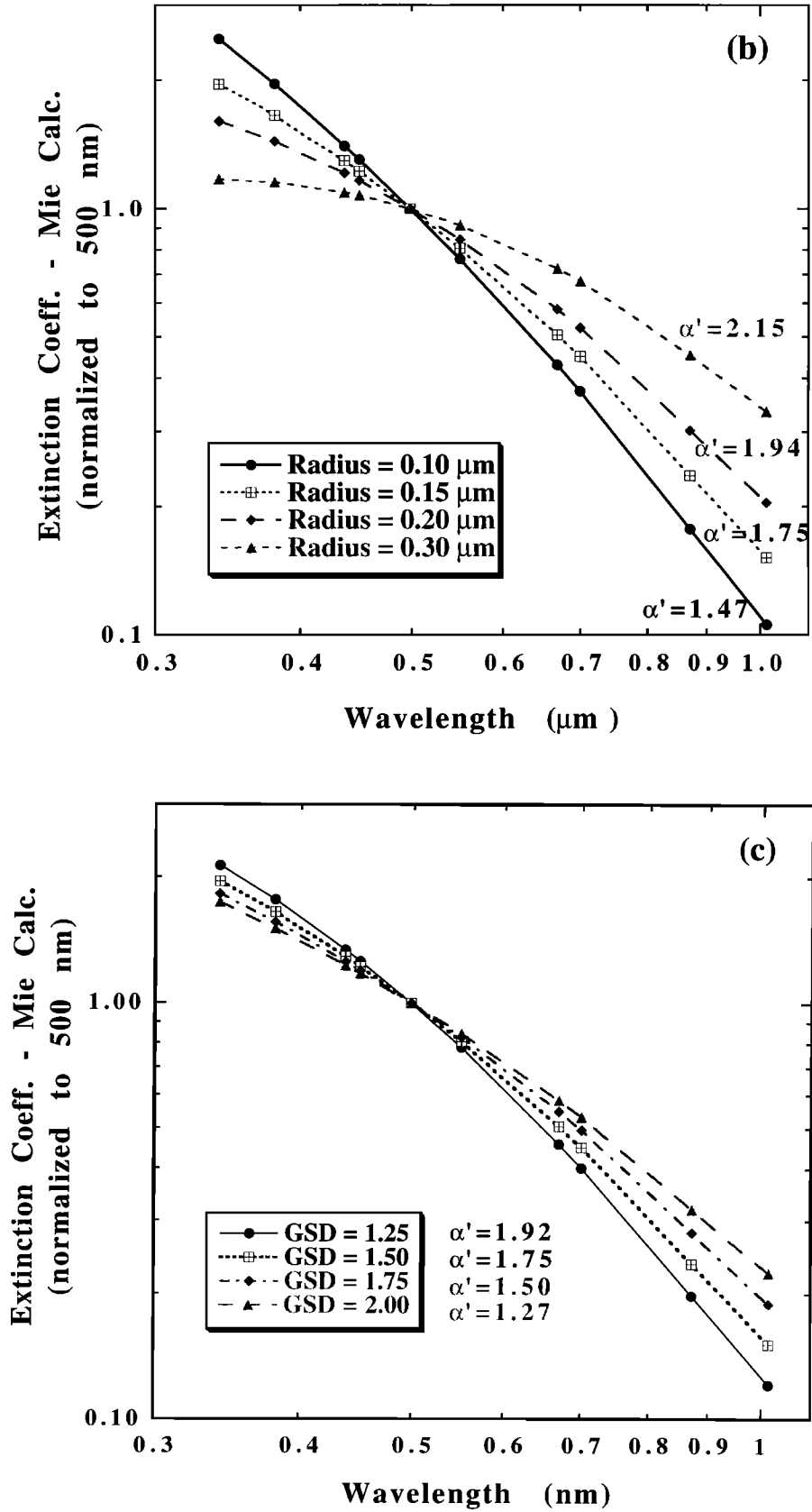


Figure 13. (continued)

information include comparisons of satellite to ground-based measurements of τ_a and for wavelength extrapolation of measured data for use in flux and energy balance calculations.

5. Summary and Conclusions

Measurements of spectral aerosol optical depth and directional sky radiances were made with AERONET Sun-sky radiometers in western Zambia in August–September 1997 in order to characterize the optical properties of African savanna biomass burning aerosols during the peak period of the burning season. The principal findings of our study are summarized as follows:

1. A high correlation between τ_a and PWV ($r^2=0.76$) during this time period suggests smoke transport from areas that have high PWV. TOMS satellite aerosol retrievals in conjunction with streamline analysis at 700 mbar show a northerly flow component associated with high τ_a and PWV. However, this correlation may also be due in part to aerosol hygroscopic growth at higher relative humidity.

2. Analysis of the τ_a spatial variance from Sun photometers located in a north–south transect in western Zambia shows a gradient in τ_a , with higher values in the north probably due in part to a greater vegetation density in the north (more fuel to burn) as a result of the north–south annual rainfall gradient.

3. Size distribution retrievals of African savanna biomass burning smoke show that the accumulation mode particles (radius $< 0.5 \mu\text{m}$) dominate with particle size increasing as optical depth increases. Comparison to biomass burning smoke from forested regions of Amazonia show that African savanna smoke is smaller in size at the same optical depth (by $\sim 0.035 \mu\text{m}$ at $\tau_{a440} = 0.68$, Figure 6), possibly due to a lower fuel moisture content and a greater percentage of flaming versus smoldering combustion. Another factor that may have contributed to the observed difference in size is the distance and speed of transport and the resultant aging of the aerosol that may also have differed for these sites.

4. The single-scattering albedo of the sampled African savanna smoke was relatively low, with mean values retrieved at $\sim 550 \text{ nm}$ from several techniques ranging from ~ 0.82 to 0.85 . There was little change in ω_0 as a function of τ_a , for τ_{a440} ranging from 0.7 to 1.7 , thus suggesting a weak effect of aging or aerosol concentration on the magnitude of ω_0 . These values of ω_0 are significantly lower than values measured for forested regions in Amazonia, probably due in part to a higher percentage of flaming phase combustion in African savannas producing a greater percentage of black carbon. The spectral change in ω_0 for African savanna smoke is quite large, with values at 440 nm of ~ 0.89 and at 1020 nm of ~ 0.79 .

5. The Ångström wavelength exponent (α) exhibited significant spectral differences due to the dominance of accumulation mode particles in the size distribution. The short wavelength computed α values (for example computed from the 380 and 500 nm wavelength pair) were much more sensitive to accumulation mode particle size, which was shown by Reid et al., [1999] for Amazonian biomass burning aerosols. However, α computations that contain longer wavelengths were more sensitive to the change in relative magnitude between the accumulation mode and the coarse mode. The departure from linearity of the $\ln \tau_a$ versus $\ln \lambda$ relationship for accumulation mode dominated size

distributions was found to be sensitive to the particle size within the accumulation mode and to the magnitude of absorption. This resulted in a smaller degree of non-linearity (smaller α') for the African savanna smoke versus mid-Atlantic United States haze due to the African smoke having smaller-size particles and greater absorption.

It is noted that the aerosol optical properties of African savanna biomass burning aerosols presented in this paper are representative of the region of western Zambia. It is not known if or how the optical properties of biomass burning aerosols from other savanna regions of Africa may differ from these. In August–September 2000 a large internationally coordinated field experiment called SAFARI 2000 was conducted in southern Africa which focussed in part on biomass burning aerosols and which will result in a more thorough understanding of these aerosols.

Acknowledgments. This project was supported by Mike King, EOS Project Office. We acknowledge the critical efforts of Nader Abuhassen and Wayne Newcomb in maintaining and adjusting the radiometers deployed in the AERONET network. We also thank the reviewers for their thoughtful comments and suggestions, which helped in improving the manuscript.

References

- Ångström, A., On the atmospheric transmission of Sun radiation and on dust in the air, *Geogr. Ann.*, **12**, 130–159, 1929.
- Bird, R.E., and C. Riordan, Simple solar spectral model for direct and diffuse irradiance on horizontal and tilted planes at the Earth's surface for cloudless atmospheres, *J. Clim. Appl. Meteorol.*, **25**, 87–97, 1986.
- Christopher, S.A., X. Li, R. M. Welch, J. S. Reid, P. V. Hobbs, T. F. Eck, and B.N. Holben, Estimation of surface and top-of-atmosphere shortwave irradiance in biomass burning regions during SCAR-B", *J. Appl. Meteorol.*, in press, 2000.
- Cooke, W.F., B. Koffi, and J.-M. Gregoire, Seasonality of vegetation fires in Africa from remote sensing data and application to a global chemistry model, *J. Geophys. Res.*, **101**, 21,051–21,065, 1996.
- Deering, D.W., Field measurements of bidirectional reflectance, chap. 2 in *Theory and Applications of Optical Remote Sensing*, edited by G. Asrar, John Wiley, New York, 1989.
- Dubovik O., A. Smirnov, B. N. Holben, M. D. King, Y. J. Kaufman, T. F. Eck, and I. Slutsker, Accuracy assessments of aerosol optical properties retrieved from AERONET Sun and sky-radiance measurements, *J. Geophys. Res.*, **105**, 9791–9806, 2000.
- Dwyer, E., J.-M. Gregoire, and J.-P. Malingreau, A global analysis of vegetation fires using satellite images: Spatial and temporal dynamics, *Ambio*, **27**, 175–181, 1998.
- Eck, T.F., B.N. Holben, I. Slutsker, and A. Setzer, Measurements of irradiance attenuation and estimation of aerosol single-scattering albedo for biomass burning aerosols in Amazonia, *J. Geophys. Res.*, **103**, 31,865–31,878, 1998.
- Eck, T.F., B.N. Holben, J.S. Reid, O. Dubovik, A. Smirnov, N.T. O'Neill, I. Slutsker, and S. Kinne, Wavelength dependence of the optical depth of biomass burning, urban, and desert dust aerosols, *J. Geophys. Res.*, **104**, 31,333–31,349, 1999.
- Garstang, M., P.D. Tyson, R. Swap, M. Edwards, P. Kallberg, and J.A. Lindsay, Horizontal and vertical transport of air over southern Africa, *J. Geophys. Res.*, **101**, 23,721–23,736, 1996.
- Goldammer, J.G., Tropical wild-land fires and global changes: Prehistoric evidence, present fire regimes, and future trends, in *Global Biomass Burning: Atmospheric, Climatic, and Biospheric Implications*, edited by J.S. Levine, pp. 83–91, MIT Press, Cambridge, Mass., 1991.
- Guild, L.S., J.B. Kauffman, L.J. Ellingson, D. L. Cummings, E.A. Castro, R.E. Babbitt, and D.E. Ward, Dynamics associated with total aboveground biomass, C, nutrient pools, and biomass burning of primary forest and pasture in Rondonia, Brazil, during SCAR-B, *J. Geophys. Res.*, **103**, 32,091–32,100, 1998.

- Hansen, J., M. Sato, and R. Ruedy, Radiative forcing and climate response, *J. Geophys. Res.*, **102**, 6,831-6,864, 1997.
- Herman, J.R., P.K. Bhartia, O. Torres, C. Hsu, C. Seftor, and E. Celarier, Global distribution of UV-absorbing aerosols from Nimbus 7/TOMS data, *J. Geophys. Res.*, **102**, 16,911-16,922, 1997.
- Holben, B.N., et al., AERONET - A federated instrument network and data archive for aerosol characterization, *Remote Sens. Environ.*, **66**, 1-16, 1998.
- Holben, B.N. et al., An emerging ground-based aerosol climatology: Aerosol optical depth from AERONET, *J. Geophys. Res.*, in press, 2001.
- Hsu, N.C., J.R. Herman, O. Torres, B.N. Holben, D. Tanre, T.F. Eck, A. Smirnov, B. Chatenet, and F. Lavenu, Comparisons of the TOMS aerosol index with Sun photometer aerosol optical thickness: Results and applications, *J. Geophys. Res.*, **104**, 6269-6279, 1999.
- Justice, C.O., T.F. Eck, D. Tanre, and B.N. Holben, The effect of water vapor on the normalized difference vegetation index derived for the Sahelian region from NOAA AVHRR data, *Int. J. Remote Sens.*, **12**, 1165-1187, 1991.
- Justice, C. O., J. D. Kendall, P.R. Dowtry, and R.J. Scholes, Satellite remote sensing of fires during the SAFARI campaign using NOAA advanced very high resolution radiometer data, *J. Geophys. Res.*, **101**, 23,851-23,863, 1996.
- Kaufman, Y.J., D. Tanre, H.R. Gordon, T. Nakajima, J. Lenoble, R. Frouin, H. Grassl, B.M. Herman, M.D. King, and P.M. Teillet, Passive remote sensing of tropospheric aerosol and atmospheric correction for the aerosol effect, *J. Geophys. Res.*, **102**, 16,815-16,830, 1997.
- Kaufman, Y.J., et al., Smoke, Clouds, and Radiation-Brazil (SCAR-B) experiment, *J. Geophys. Res.*, **103**, 31,783-31,808, 1998.
- King, M.D., Y.J. Kaufman, D. Tanre, and T. Nakajima, Remote sensing of tropospheric aerosols from space: Past, present, and future, *Bull. Am. Meteorol. Soc.*, **80**, 2229-2259, 1999.
- Kinne, S., T.P. Ackerman, M. Shiobara, A. Uchiyama, A.J. Heymsfield, L. Miloshevich, J. Wendell, E.W. Eloranta, C. Purgold, and R.W. Bergstrom, Cirrus cloud radiative and microphysical properties from ground observations and in situ measurements during FIRE 1991 and their application to exhibit problems in cirrus solar radiative transfer modeling, *J. Atmos. Sci.*, **54**, 2320-2344, 1997.
- Konzelmann, T., D.R. Cahoon, and C.H. Whitlock, Impact of biomass burning in equatorial Africa on the downward surface shortwave solar irradiance: Observations versus calculations, *J. Geophys. Res.*, **101**, 22,833-22,844, 1996.
- Kotchenruther, R., and P.V. Hobbs, Humidification factors of aerosols from biomass burning in Brazil, *J. Geophys. Res.*, **103**, 32,081-32,090, 1998.
- Kotchenruther, R., P.V. Hobbs, and D.A. Hegg, Humidification factors for atmospheric aerosols off the mid-Atlantic coast of the United States, *J. Geophys. Res.*, **104**, 2239-2251, 1999.
- Lenoble, J., The particulate matter from biomass burning: A tutorial and critical review of its radiative impact, chap. 46 in *Global Biomass Burning: Atmospheric, Climatic, and Biospheric Implications*, edited by J.S. Levine, pp. 381-386, MIT Press, Cambridge, Mass., 1991.
- Levine, J.S., W.R. Cofer III, D.R. Cahoon Jr., and E.L. Winstead, Biomass burning - A driver for global change, *Environ. Sci. Technol.*, **29**, 120A-125A, 1995.
- Li, Y., T.H. Demetriades-Shah, E.T. Kanemasu, J.K. Shultis, and M.B. Kirkam, Use of second derivatives of canopy reflectance for monitoring prairie vegetation over different soil backgrounds, *Remote Sens. Environ.*, **44**, 81-87, 1993.
- Liousse, C., C. Devaux, F. Dulac, and H. Cachier, Aging of savanna biomass burning aerosols: consequences on their optical properties, *J. Atmos. Chem.*, **22**, 1-17, 1995.
- Markham, B.L., J.S. Schafer, B.N. Holben, and R.N. Halthore, Atmospheric aerosol and water vapor characteristics over north central Canada during BOREAS, *J. Geophys. Res.*, **102**, 29,737-29,745, 1997.
- Martins, J.V., P.V. Hobbs, R.E. Weiss, and P. Artaxo, Sphericity and morphology of smoke particles from biomass burning in Brazil, *J. Geophys. Res.*, **103**, 32,051-32,057, 1998.
- Mims, F.M. III, An international haze-monitoring network for students, *Bull. Am. Meteorol. Soc.*, **80**, 1421-1431, 1999.
- Neckel, H., and D. Labs, Improved data of solar spectral irradiance from 0.33 to 1.25 μm , *Solar Phys.*, **74**, 231-249, 1981.
- O'Neill, N.T., T.F. Eck, B.N. Holben, A. Smirnov, O. Dubovik, and A. Royer, Uni and bimodal size distribution influences on the variation of Ångström derivatives in spectral and optical depth space, *J. Geophys. Res.*, in press, 2000.
- Reid, J.S., and P.V. Hobbs, Physical and optical properties of young smoke from individual biomass fires in Brazil, *J. Geophys. Res.*, **103**, 32,013-32,031, 1998.
- Reid, J.S., P.V. Hobbs, R.J. Ferek, D.R. Blake, J.V. Martens, M.R. Dunlap, and C. Liousse, Physical, chemical, and optical properties of regional hazes dominated by smoke in Brazil, *J. Geophys. Res.*, **103**, 32,059-32,080, 1998a.
- Reid, J.S., P.V. Hobbs, C. Liousse, J. Vanderlei Martins, R.E. Weiss, and T.F. Eck, Comparisons of techniques for measuring shortwave absorption and the black carbon content of aerosols from biomass burning in Brazil, *J. Geophys. Res.*, **103**, 32,031-32,040, 1998b.
- Reid, J.S., T.F. Eck, S.A. Christopher, P.V. Hobbs, and B.N. Holben, Use of the Ångström exponent to estimate the variability of optical and physical properties of aging smoke particles in Brazil, *J. Geophys. Res.*, **104**, 27,473-27,489, 1999.
- Remer, L.A., and Y.J. Kaufman, Dynamic aerosol model: Urban/industrial aerosol, *J. Geophys. Res.*, **103**, 13,859-13,871, 1998.
- Remer, L.A., Y. Kaufman, B.N. Holben, A.M. Thompson, and D.P. McNamara, Biomass burning aerosol size distribution and modeled optical properties, *J. Geophys. Res.*, **103**, 31,879-31,891, 1998.
- Schmid, B., J. Michalsky, R. Halthore, M. Beauharnois, L. Harrison, J. Livingston, P. Russell, B. Holben, T. Eck, and A. Smirnov, Comparison of aerosol optical depth from four solar radiometers during the fall 1997 ARM intensive observation period, *Geophys. Res. Lett.*, **26**, 2725-2728, 1999.
- Scholes, C. O., J. D. Kendall, and C. O. Justice, The quantity of biomass burned in southern Africa, *J. Geophys. Res.*, **101**, 23,667-23,676, 1996.
- Smirnov, A., B.N. Holben, T.F. Eck, O. Dubovik, and I. Slutsker, Cloud screening and quality control algorithms for the AERONET data base, *Remote Sens. Environ.*, **73**, 337-349, 2000a.
- Smirnov, A., B.N. Holben, O. Dubovik, N.T. O'Neill, L.A. Remer, T.F. Eck, I. Slutsker, and D. Savoie, Measurement of atmospheric optical parameters on U.S. Atlantic coast sites, ships, and Bermuda during TARFOX, *J. Geophys. Res.*, **105**, 9887-9901, 2000b.
- Vermote, E., D. Tanre, J.L. Deuze, M. Herman, and J.J. Morcrette, Second simulation of the satellite signal in the solar spectrum, 6S: An overview, *IEEE Trans. Geosci. Remote Sens.*, **35**, 675-686, 1997.
- Ward, D. E., R. A. Susott, J. B. Kaufman, R. E. Babbitt, D. L. Cummings, B. Dias, B.N. Holben, Y. J. Kaufman, R. A. Rasmussen, and A. W. Setzer, Smoke and fire characteristics for cerrado and deforestation burns in Brazil: Base-B experiment, *J. Geophys. Res.*, **97**, 14,601-14,619, 1992.
- Ward, D. E., W. M. Hao, R. A. Susott, R. E. Babbitt, R. W. Shea, J. B. Kaufman, and C. O. Justice, Effect of fuel composition on combustion efficiency and emission factors for African savanna ecosystems, *J. Geophys. Res.*, **101**, 23,569-23,576, 1996.
- Wild, M., Discrepancies between model-calculated and observed shortwave atmospheric absorption in areas with high aerosol loadings, *J. Geophys. Res.*, **104**, 27,361-27,371, 1999.
- O. Dubovik, N.C. Hsu, I. Slutsker, and A. Smirnov, Science Systems and Applications, Inc., Code 923, NASA Goddard Space Flight Center, Greenbelt, MD 20771. (dubovik@aeronet.gsfc.nasa.gov; hsu@wrabbit.gsfc.nasa.gov; asmirnov@aeronet.gsfc.nasa.gov; ilya@aeronet.gsfc.nasa.gov)
- T.F. Eck, GEST Center, Code 923, NASA Goddard Space Flight Center, Greenbelt, MD 20771. (tom@aeronet.gsfc.nasa.gov)
- B.N. Holben, Biospheric Sciences Branch, Code 923, NASA Goddard Space Flight Center, Greenbelt, MD 20771. (brent@aeronet.gsfc.nasa.gov)
- M.M. Mukelabai, Zambian Meteorological Department, Mongu, Zambia. (mmuke@zamnet.zm)
- N.T. O'Neill, CARTEL, Université de Sherbrooke, Sherbrooke, Quebec, Canada, J1K 2R1. (noneill@courrier.usherb.ca)
- J.S. Reid, SPAWARSCEN SAN DIEGO D858, 49170 Propagation Path, San Diego, CA 92152-7385. (jreid@spawar.navy.mil)
- D.E. Ward, Intermountain Research Station, USDA Forest Service, Missoula, MT 59807. (pyroward@aol.com)

(Received April 6, 2000; revised July 25, 2000;
accepted August 29, 2000)